Bending and wrinkling of composite fiber preforms and prepregs. A review and new developments in the draping simulations

Philippe Boissé, Julien Colmars, Nahiene Hamila, Naïm Naouar, Quentin Steer

Bending and wrinkling of composite fiber preforms and prepregs. A review and new developments in the draping simulations

P. Boisse*, J. Colmars, N. Hamila, N. Naouar, Q. Steer

Université de Lyon, LaMCoS, INSA, Lyon, F-69621, France

Bending properties play a significant role in the forming of textile composites reinforcements, particularly in determining the shape of wrinkles. The physics related to the bending of fibrous reinforcements is specific. Bending is due to slippage between the fibers and since the fibers are quasi-inextensible, standard plate and shell theories are irrelevant. To measure bending characteristics, three experimental tests (and their variants) have been developed in the last decades, and efforts are currently devoted to extending and improving these tests. From their results, simulations can be performed by introducing a flexural energy related to the bending moment and the curvature. In particular, wrinkles during forming can be simulated. In the case of 3D modeling of thick reinforcements, the use of generalized continuum mechanics model is necessary because of the bending stiffness of each fiber and the slippage between fibers. In order to simulate textile reinforcements with shells, some shell approaches, different of the standard theories, can correctly calculate the rotations of textile reinforcement normals.

1. Introduction

Textile composites make it possible to produce parts with good performances and low mass, and consequently various sectors in the industry, especially aeronautics industry, have developed new products made of composites [1–3]. Composite manufacturing processes are numerous and often complex. They frequently include a forming stage of dry textile reinforcements (in Liquid Molding Processes (LCM) [4,5]) or preimpregnated textile reinforcements [6–9]. The development of high-quality forming processes is necessary but can be difficult. Numerical simulations of the composite forming process can give an initial validation of the feasibility of the process and a determination of suitable parameters. This helps avoid a time-consuming and costly "trial and error" development.

The simulation of the textile reinforcement (or prepreg) forming process requires the knowledge and the modeling of the textile reinforcement's thermomechanical behavior. During the process, the matrix is either absent (in LCM processes, it is injected afterwards) or melted (due to heating above the melt temperature of the prepreg). Some deformation modes of the reinforcement during the composite forming are specific and render forming possible. A significant effort has been made over the last two decades to model this mechanical behavior in order to simulate the forming process.

The textile reinforcements are made up of fibers with very small diameters (5 or 7 μm for a carbon fiber). The fibers are quasi-inextensible and bonded by weaving (or braiding, knitting, stitching …). Movements are nevertheless possible between fibers due to the relative slippage. These two points, i.e., the quasi-inextensibility and possible slippage between fibers, are the two main reasons for the very specific mechanical behavior of fibrous reinforcements. When it comes to prepregs, their mechanical behavior is of the same nature because the resin is melted during forming and does not change the deformation modes. The relative slippage between fibers leads to a much lower bending stiffness than for continuous materials such as metals or polymers. Classical plate and shell theories do not apply (in their standard form) and there is no direct relation between the bending stiffness and that of tension as there is for plates made of continuous materials. This weak bending stiffness facilitates the forming and reduces the loads during the process. Large curvatures can be obtained without damage of the textile reinforcement. On the other hand, wrinkling of the fibrous reinforcements is frequent because of the slippage between fibers and the consequent low bending stiffness.

Forming simulations for textile composite reinforcements (often called draping simulations) were first carried out with a membrane hypothesis, i.e., neglecting the bending stiffness [10–15]. However, it has been shown that the simulation of wrinkles during textile reinforcement forming needs a shell approach which takes into account the bending stiffness [16–18]. The analysis of wrinkles is linked to the

* Corresponding author. INSA avenue Jean Capelle, 69621 Villeurbanne, France.
E-mail address: philippe.boisse@insa-lyon.fr (P. Boisse).

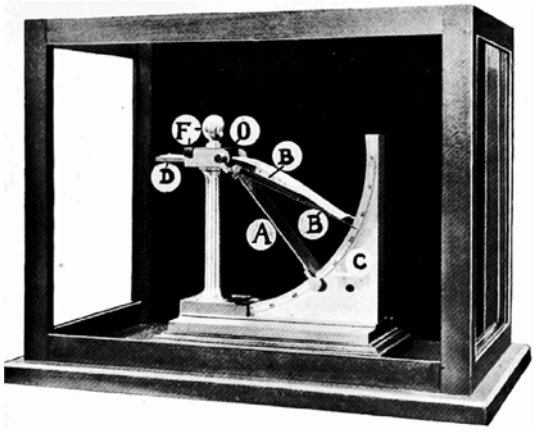

Fig. 1. Peirce flexometer [29].

bending behavior since their number and size depend on the bending stiffness. The fibrous nature and the architecture of the weaving (or stitching/braiding) condition all the mechanical behaviors of the reinforcement. The tensile behavior depends on the crimp and on the weave between warp and weft yarns [19–22].

Much experimental and modeling work has concerned and still concerns in-plane shear [23–28]. The bending of textile materials has been a topic of research studies for the past hundred years. The Peirce method was developed in the 1930's [29,30], and is based on the cantilever bending of a textile specimen under its own weight (Fig. 1). It is noteworthy that this method is still widely used today. Its utilization is specified in several standards [31–33]. This method assumes that the bending moment has a linear dependence on the curvature, as detailed below in Section 3. The Kawabata bending test (KES-F2) (Fig. 2) makes it possible to obtain a loading cycle and shows that the bending behavior is generally not linear [34]. Grosberg's model provides the possibility of taking friction into account by introducing a threshold moment which must be exceeded in order for the curvature to vary [35]. The Dahl model [36] is a generalization of the Coulomb friction model. It makes it possible to take into account the friction and to obtain a moment-curvature curve that is more realistic on a cycle than the Grosberg's model [37]. Extensions of these models have been developed in Refs. [38,39] with the aim to take into account the viscosity and the Stribeck effect (characterized by decreasing friction with respect to low velocities) [38,40].

The main bending tests and methods of analysis are presented in Section 3 as well as the extensions of these methods to high-temperature measurements required in the case of prepregs. The experimental methods cited above aim to determine the relation between the bending moment and the curvature. A plate or shell theory also provides the kinematics for the points situated in the thickness [41–43]. However, kinematics in the thickness of the textile reinforcements is very specific in view of the quasi-inextensibility of the fibers and the possible relative slippage.

Many of the draping simulations are currently based on shell finite elements with the objective of determining the deformation of the mean surface and in particular wrinkles and in-plane shear angles [44–52]. The kinematics through the thickness is generally not considered.

Section 4 gives a presentation of the simulation of the wrinkling onset and the developments during the draping of the textile reinforcements. The influence of the different rigidities and especially the bending stiffness on the wrinkles is analyzed. The concept of a locking angle is questioned.

In some cases and in particular when simulating the forming of 3D reinforcements whose thickness may be significant, it is necessary to determine strains and stresses throughout the thickness of the reinforcement. To obtain a result in the most general case, a 3D simulation can be performed. Section 5 shows that the analysis of bending of textile reinforcements by 3D finite elements leads to difficulties when using a behavior law involving the standard continuum mechanics of Cauchy [53,54]. Generalized Continuum Mechanics approaches [55,56] make it possible to overcome some difficulties in material modeling. It will be shown in section 5 that a second gradient model can lead to correct 3D simulations for the bending of the textile

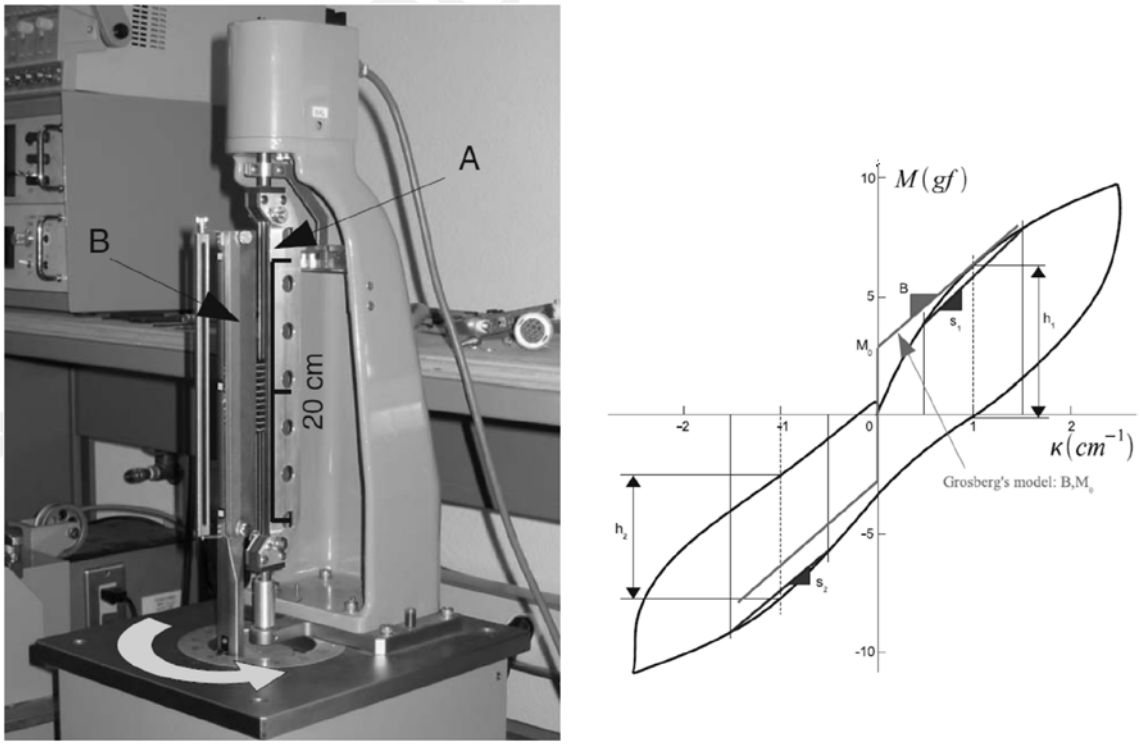

Fig. 2. Kawabata bending test - KES-FB2, experimental curve and Grosberg model [64].

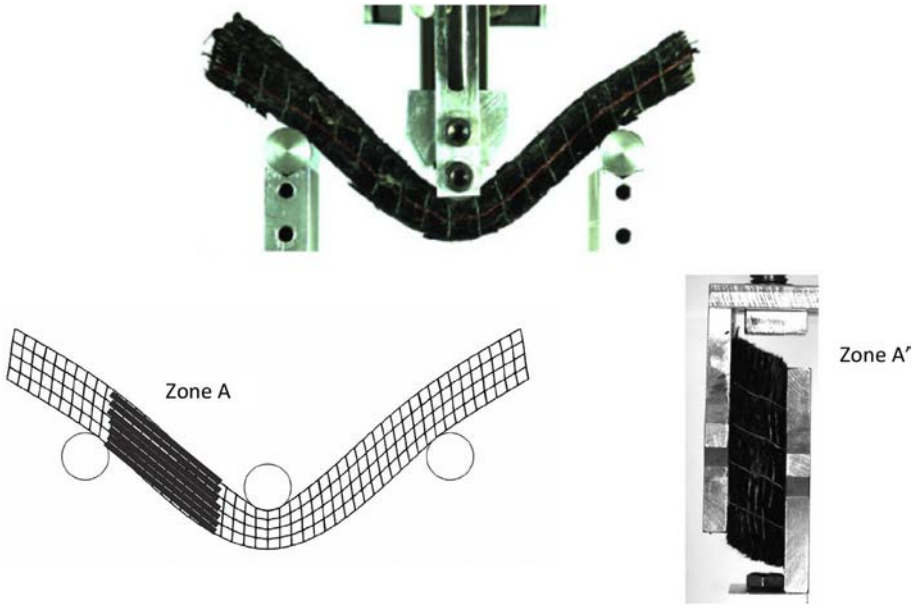

Fig. 3. Shear deformation of a reinforcement during bending.

reinforcements. Finally, section 6 presents a shell formulation for simulations of the forming of fibrous reinforcements which correctly models their kinematics and the deformation of the points in their thickness [57].

It should be underlined that the research in the field of the present subject is currently very active. A large part of the articles in reference are from 2016 to 2017.

2. Taking into account bending behavior when analyzing the forming of textile reinforcements

2.1. Reasons for the specific bending behavior of textile reinforcements

The bending stiffness of fibrous material, especially of composite textile reinforcements, is weak. In membrane approaches [10–15,58] and in kinematic approaches (based on the fishnet algorithm) [59–61], the bending stiffness is neglected. The fact that the textile bending stiffness is so weak is due to possible slippage between the fibers. Fig. 3 shows a three-point bending of a textile interlock reinforcement. The bending of the specimen is principally due to the slippage between the fibers. When the textile reinforcement is considered as a continuous medium, this deformation is a shear strain. The deformation of zone A (Fig. 3) is of the same nature as that of zone A′ in a shear test. The possible slippage leads to a weak shear stiffness when the fibrous reinforcement is seen as a continuous medium and consequently the bending stiffness of the reinforcement when seen as a plate or a shell is also low.

The inextensibility (or quasi-inextensibility) of the fibers is the second specificity of the mechanical behavior of fiber reinforcements. In a bending test such as that shown in Fig. 3, the inextensibility fixes the position of the material sections initially perpendicular to the mean surface. These material sections do not remain perpendicular in the deformed state. The kinematics of the fibrous materials based on possible slippage between fibers and fiber inextensibility do not correspond to the assumptions of standard plate theories (Kirchhoff, Mindlin). For a continuous material (such as a metal sheet), plate theories lead to membrane and bending rigidities that are linked and can be calculated from the elastic properties of the material and the plate geometry. For textile reinforcements such an approach would lead to excessive bending stiffness because slippage between fibers is not taken into account in standard plate theories. Consequently it is not possible to use standard shell finite elements available in commercial software in which the bending rigidity is calculated from the tensile modulus and standard shell theories. To carry out a correct analysis, the fibrous reinforcement analyses can be done by decoupling the membrane and bending behaviors [44,62].

2.2. Decoupling the membrane and bending behaviors. Analysis of the mean surface bending

In order to improve the membrane approaches, the bending deformation energy can be added and decoupled from that of the membrane by considering a moment-curvature relation that is independent of the membrane deformations. The virtual work theorem relates, i.e., the internal, exterior and acceleration virtual works respectively. In any virtual displacement field $\boldsymbol{\eta}$ such as $\boldsymbol{\eta} = 0$ on the boundary with prescribed displacements, we have:

$$W_{ext}(\boldsymbol{\eta}) - W_{int}(\boldsymbol{\eta}) = W_{acc}(\boldsymbol{\eta}) \tag{1}$$

The internal virtual work can be assumed to be separated into:

$$W_{int}(\boldsymbol{\eta}) = W_{int}^{memb}(\boldsymbol{\eta}) + W_{int}^{bend}(\boldsymbol{\eta}) \tag{2}$$

where $W_{int}^{memb}(\boldsymbol{\eta})$ is the virtual work of membrane and $W_{int}^{bend}(\boldsymbol{\eta})$ is the virtual work of bending with:

$$W_{int}^{bend}(\boldsymbol{\eta}) = \int_S \chi_{11}(\boldsymbol{\eta})M^{11} + \chi_{22}(\boldsymbol{\eta})M^{22}dS \tag{3}$$

Here, χ_{11} and χ_{22} are the curvatures in the warp and weft directions. The bending moments in the warp and weft directions are assumed to be in the form $M^{11}(\chi_{11})$, $M^{22}(\chi_{22})$, The twisting virtual work $\chi_{12}(\boldsymbol{\eta})M^{12}$ is neglected. It can be added if the twisting stiffness is important (and if experimental data exist).

This approach requires the membrane properties of the textile reinforcement (tension and in-plane shear) and the bending moments as a function of the curvature. The latter property is given directly by the experimental devices presented in Section 3. This approach is implemented in a rotation-free three-node shell element [44] to simulate textile reinforcement forming. Fig. 4 shows the simulation of the deep drawing of a tetrahedral shape and the comparison with the forming experiment. The shear angles but also the wrinkles are in good agreement [46]. This approach is used in Section 4 to analyze wrinkling simulations.

Nevertheless, the approach presented above (as well as most of all current methods taking bending stiffness into account in textile reinforcement forming) does not give the distribution of displacements

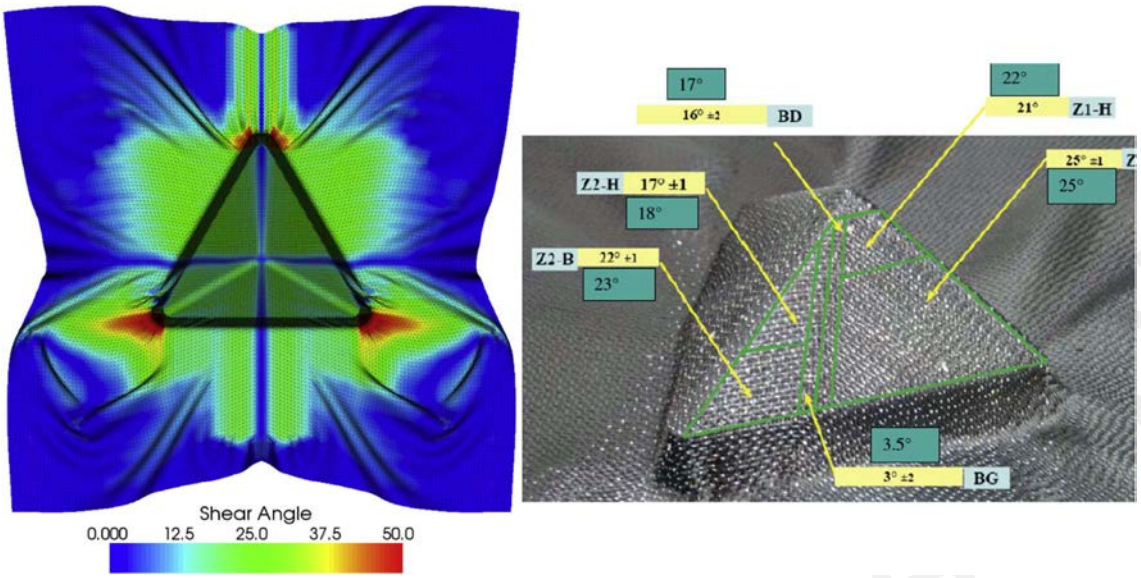

Fig. 4. Tetrahedral forming. Comparison of simulation and experiments [46].

and strains in the thickness. For some analyses, shear angles and wrinkle shapes are sufficient. If strain and stresses in the thickness are required, a 3D approach (see Section 5) or a specific shell formulation for fibrous reinforcements must be used (see Section 6).

3. Experimental methods for measuring the bending property

To introduce bending in the modeling of a textile reinforcement deformation by shell elements, the relation between the bending moment and the curvature M(χ) is the characteristic whose knowledge is necessary.

3.1. Peirce cantilever test

This method [29] and its variants and extensions have been introduced in 1930 by F.T. Peirce and are still in use [31–33]. The test is based on the cantilever bending of a textile specimen subjected to its own weight. The specimen is progressively advanced until the free end makes contact with the inclined plane of the device (Fig. 5). The position of a point of the midline of the textile specimen is located in (x,y) (Fig. 5). w is the weight per unit length and ℓ is the overhanging length of the specimen The relation between the bending moment M and the curvature χ is assumed to be linear. (This is a main assumption of the Peirce's approach):

$$M = G\chi \tag{4}$$

where G is the bending stiffness assumed to be constant. For small deflections, y' is small and the curvature

$$\chi = \frac{y''}{(1 + y'^2)} \tag{5}$$

can be approximated by $\chi = y''$. The bending moment in a section of the textile specimen is:

$$M = \frac{w}{2}(\ell - x)^2. \tag{6}$$

Replacing the bending moment (Eq. (6)) and the curvature $\chi = y''$, in Eq. (4), a differential equation of the deflection is obtained:

$$Gy'' = \frac{w}{2}(\ell - x)^2 \tag{7}$$

By integrating twice and taking into account the boundary conditions y (0) = y '(0) = 0, the deflection δ at the free end is obtained:

$$\delta = y(\ell) = \frac{w\ell^4}{8G} \tag{8}$$

An inclined plane passing through the free end after deformation A (Fig. 5) and the clamping point B is considered. It is oriented relative to the horizontal by the angle θ. The flexural rigidity $S = \frac{G}{w}$ is expressed in function of θ:

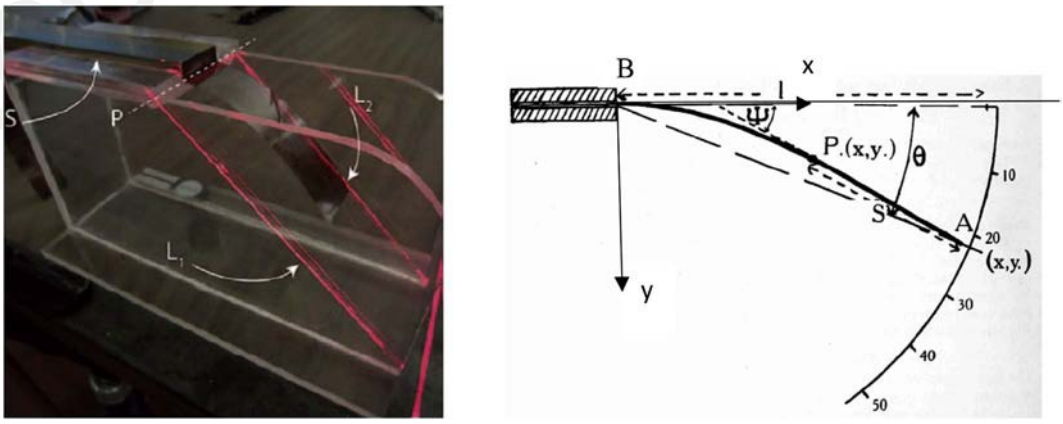

Fig. 5. Peirce's Cantilever bending test [29,63].

Fig. 6. Standard cantilever bending test with an inclined plane at 41.5°.

$$S = \frac{G}{w} = \frac{\ell^3}{8tg\theta} \tag{9}$$

For large deflections, Peirce introduces a corrective term function:

$$S = \frac{G}{w} = \frac{\ell^3 \cos\theta/2}{8tg\theta} \tag{10}$$

Consequently, the flexural rigidity S and the bending stiffness G are determined by Eq. (10) from the measurement of the overhanging length ℓ for a given angle of inclination θ.

In the standard commercial device (Fig. 6), the inclined plane is fixed at θ = 41.5°. With this angle:

$$S = \frac{G}{w} \approx \frac{\ell}{8} \tag{11}$$

The correction by cosθ/2 in the case of large deflections (Eq. (10)) is empirical. However, it can be validated by a finite element analysis of a specimen bending. Table 1 compares, for the same given weight w) the angle θ obtained by the Peirce equation (10) to the angle θ obtained by an F.E. simulation using a beam element. The two angles are close: the difference is less than 3% for angles up to 41.5°. Equation (10) (and its particular form (11) when the inclined plane is fixed at θ = 41.5° can be used in practice to determine the bending stiffness by a simple test. The Peirce test nevertheless presents a limitation. It assumes a linear bending behavior M = Gχ and provides a constant value of the bending stiffness G. Finally it should be mentioned that Lammens et al. concluded that use of the ASTM D1388 cantilever test resulted in measurements with inaccuracies [63]. The bending behavior of some textile reinforcements was non-linear as is shown in the following. The next section 3.2 presents extensions of the Peirce method which are intended to determine the bending behavior M(χ) whether the behavior is linear or not.

Table 1
Comparison between Peirce model and beam FE analysis.

Weight per unit length (N/mm)	Angle Teta (°) (Peirce)	Angle Teta (°) EF	Relative difference	Characteristics of the bending specimen	
0.00	0	0.00			
4.21E-05	6	5.98	0.274%	Thickness (mm)	0.319
8.56E-05	12	11.95	0.419%	Width (mm)	50
1.32E-04	18	17.84	0.901%	Lenght L (mm)	120
1.82E-04	24	23.56	1.849%	Bending modulus G (N.mm)	1.73
2.39E-04	30	29.36	2.128%		
3.06E-04	36	35.07	2.585%		
3.86E-04	42	40.63	3.270%		
4.87E-04	48	46.18	3.797%		
6.19E-04	54	51.75	4.162%		
8.01E-04	60	57.39	4.347%		

3.2. Cantilever bending test. Extensions of the Peirce method

Extensions of the Peirce test have been realized by De Bilbao et al. [64] and Liang et al. [65,66] with the aim of performing an optical measurement on the entire deformed shape of the specimen in flexion. The bending device developed in Ref. [64] makes it possible to vary the bending length (Fig. 7). Fig. 8 shows the principle for obtaining the Moment-Curvature curve from a single image of the deflection. The image is processed to determine the midline of the deformed specimen. The latter is approximated by an analytic curve (uniform quartic B-spline in Ref. [66]). The curve can therefore be determined at all points. The specimen is subjected to its own weight which fixes the bending moment for each section. This gives the Moment-Curvature curve by analyzing only one deflection since the moment and the curvature vary from zero at the free end up to a maximum value at the clamped end. The influence of the specimen length has been tested in Refs. [64] and [65]. The Moment-Curvature plots obtained for different lengths are fairly coherent. In order to obtain larger curvatures, required to model wrinkles in formation, an additional mass can be added at the free end of the specimen [65].

Dangora et al. [67,68] and Alshahrani et al. [69,70] developed cantilever tests in which the specimen was initially vertical. In this way, the effects of gravity were avoided (at least for small deflections).

Finally, it can be underlined that the geometry of the cantilever bending test and its free end lead to an absence of spurious tension in the specimen. This is important since the tensile stiffness is very large in comparison with its bending counterpart.

3.3. Kawabata bending test and its extensions

The Kawabata bending test (KES-FB2) and its extensions constitute the second main family of bending tests. The KES-FB2 test was developed in 1980 [34] (Fig. 9a) and involves a constant curvature imposed on a textile specimen by the rotation of one clamp. A diagram showing the principle is shown in Fig. 9b [71]. The bending moment is directly measured by the device. Fig. 2 presents the Moment-Curvature curve obtained by a Kawabata test on a carbon fabric during a loading/unloading cycle [64]. It shows a non-linear and hysteretic behavior, which is also the case for other materials tested with the Kawabata bending test [72]. Such a loading cycle is less easy to achieve with a cantilever test. Nevertheless, forming simulations do not generally require the bending behavior on a cycle. The device proposed in Refs. [71,73] (Fig. 9c) works according to the same principle as the Kawabata bending test, and uses the capabilities of a rheometer to control the temperature and bending rate.

3.4. Three-point bending test

The three-point bending test is widely used for composite material bending [74–78]. For textile reinforcements it requires the bending stiffness to be sufficiently large. It can be used for either thick enough textile reinforcements (Fig. 10a [79,82] and Fig. 10b [80]) or for small specimens. Margossian et al. used bending clamps of a Dynamic Mechanical Analysis (DMA) system to perform three-point bending tests on unidirectional thermoplastic prepregs (Fig. 10c) [81]. The specimen shown in Fig. 10c had a length of 20 mm. Such a DMA system was also used to analyze bending properties in Ref. [73]. The three-point bending test is well adapted to analyze the deformations in the thickness of the reinforcement by an optical method (Fig 10a and b) [79,80].

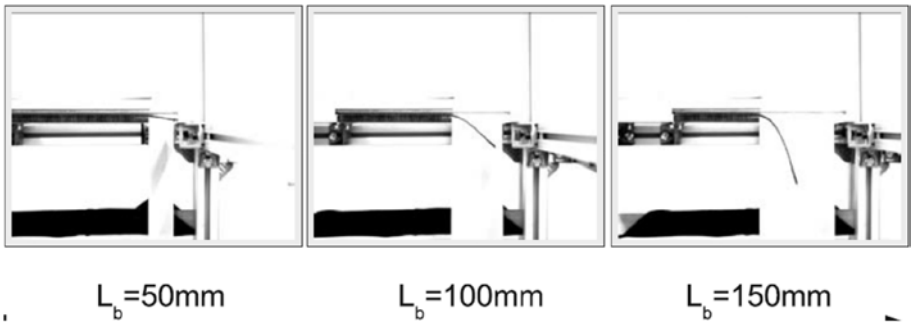

Fig. 7. Optical measurement of the deflection for different bending lengths [64].

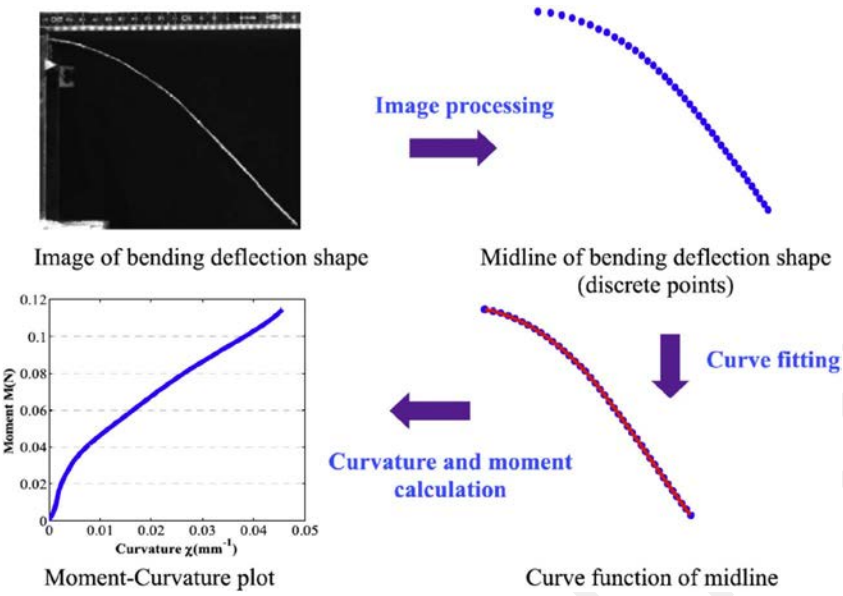

Fig. 8. Different stage of the determination of the Moment-Curvature curve from a cantilever bending test [66].

3.5. Influence of the temperature and speed

A major effort has been and is still devoted to the development of simulation of thermoforming prepregs that are either thermoset [17,50,83,84] or thermoplastic [85–94]. These processes are performed at high temperature. In particular the process of stamp forming of a thermoplastic prepreg is carried out after a pre-heating step slightly above the melting point. In the case of the PA66 matrix, the melting point is 260 °C and the thermoforming is carried out at a temperature in the region of 280 °C [90]. In the case of the PEEK matrix, the melting point is 343 °C and the thermoforming is carried out at a temperature in the region of 360 °C [87]. These temperatures concerning the PEEK matrix represent a maximum for the thermoforming of thermoplastic prepregs. Forming thermoset prepreg must be carried out at a temperature lower than the onset of cure. In the case of epoxy matrices, the temperature must remain below 100 °C. Forming is generally performed at 70 °C [69,84].

At these temperatures, the mechanical behavior and especially the bending behavior varies greatly with temperature. The bending test is realized at a set of temperatures corresponding to those that can be reached at each point during thermoforming. Different devices are used for this purpose.

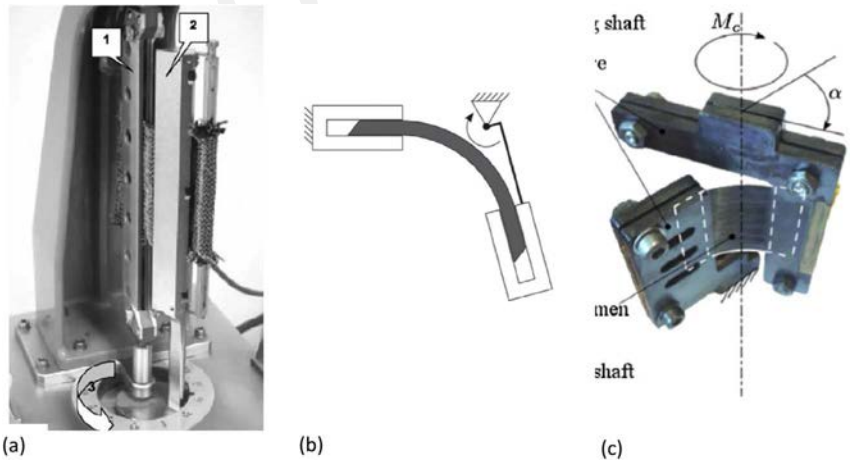

Fig. 9. Bending tests for which a constant curvature is achieved by clamp rotation. (a) Kawabata bending test [34, 72], (b) principle of the tests, (c) bending device developed in Ref. [71].

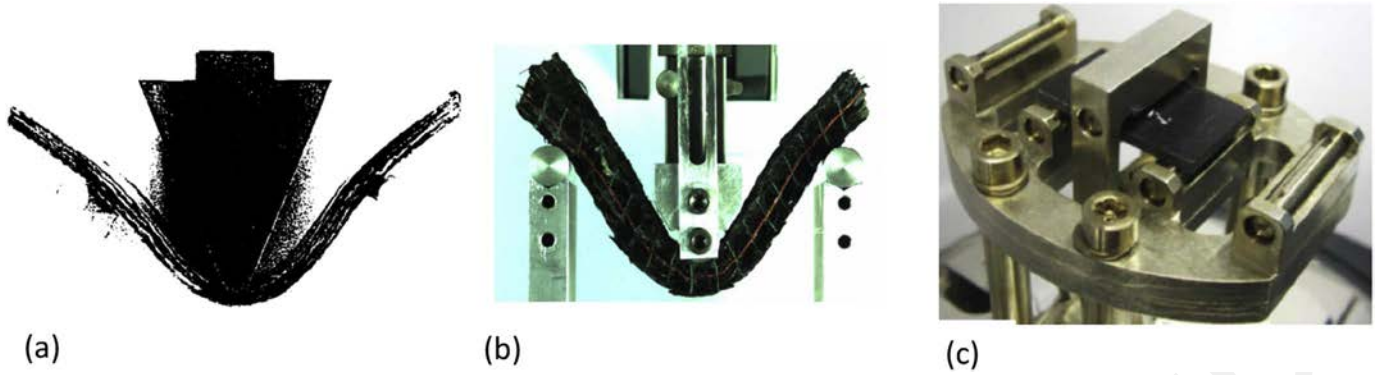

Fig. 10. Three point bending tests. (a) Bending of a preconsolidated thermoplastic sheets [82]. (b) Bending of an interlock reinforcement [80], (c) Bending of an unidirectional thermoplastic prepreg in a DMA system [81].

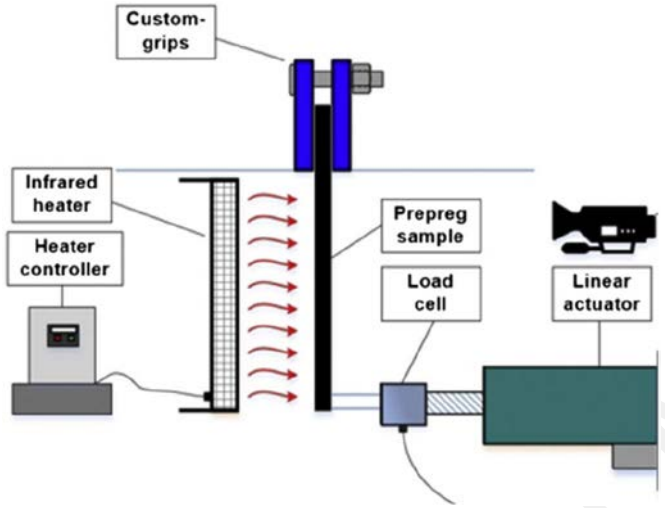

Fig. 11. Bending test at high temperature. Infrared heaters for thermoset prepregs [69].

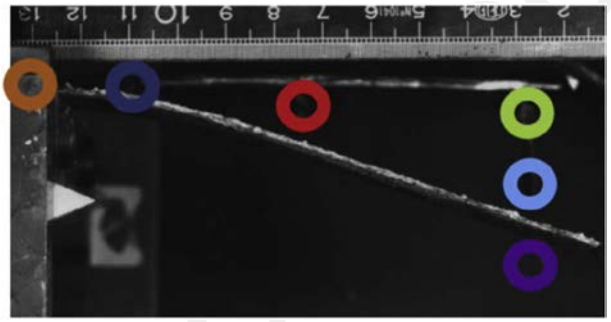

Fig. 12. Thermocouples to check the homogeneity of the temperature field inside a thermal environmental chamber during a Bending test at high temperature [65].

Fig. 11 shows the use of an infrared heater in the case of thermoset prepregs [69]. For these materials, the processing temperature remained below 100 °C. In the case of thermoforming of thermoplastic prepregs, the temperatures is generally higher: covering an interval above and below the melting temperature (343 °C for the PEEK matrix, 285 °C for the PPS matrix). A thermal environmental chamber was used, see Fig. 12. To achieve correct bending, the homogeneity of the temperature field had to be checked. This can be tricky, but it is necessary in order to get meaningful results. Fig. 12 shows the thermocouples that were used in that objective and several modifications made it possible to obtain a homogeneous temperature field [65].

The bending test presented in Ref. [71] uses the capabilities of a rheometer for temperature control. The three-point bending test developed by Margossian et al. [81] (Fig. 10c), using a Dynamic Mechanical Analysis (DMA) system, enabled analyses up to 600 °C. Infrared heating was also associated to cantilever bending in order to analyze the flexural rigidities of a cross-ply thermoplastic laminate up to 120° [68]. Fig. 13 presents two sets of bending moment-curvature plots. The first one was measured for a 5-harness carbon satin and epoxy prepreg from room temperature to 90 °C (Fig. 13a) [69] and the second one for a 5-harness carbon satin and PPS prepreg from room temperature to 300 °C (Fig. 13b) [65]. The temperature dependence was significant in both cases. Moreover, the curves were not linear.

Given the highly temperature dependent mechanical behavior of the prepregs, the thermoforming simulation must combine thermal and forming analyses [87,93,95]. Nevertheless, a large part of the present simulations assume that the prepreg is always and everywhere at the process temperature. This is a strong hypothesis that could often be questioned.

Some of the devices presented above can control the rate of the bending test. Tests carried out at different rates were thus performed to identify the parameters of the rate-dependent bending models, especially the viscoelastic ones [71,81,91,95–97]. It remains to take into account the effect of bending speed in composite forming simulations to show if this aspect is important and in which cases.

3.6. Relation between bending rigidity of yarns and fabrics

An alternative to carrying out bending tests on each textile reinforcement may be the calculation of the bending stiffness of the reinforcement from that of the yarns and the internal architecture of the fabric. A review of such approaches and some extensions are given in Refs. [98–100]. Lomov et al. presented a model based on the representation of fabric deformation as a coordinate transformation [101]. Sagar et al., proposed an approach that takes into account the compression of the yarns [102]. These approaches are compared to experimental data for different yarns and fabrics and show reasonable agreement of the models.

4. Wrinkling during forming. Influence of the bending stiffness

Wrinkles are one of the principal defects that may appear during the draping of a reinforced composite textile. They may also appear when forming other materials, in particular metals, when the thickness is small [103–107]. In the case of fibrous reinforcements, the tendency towards wrinkling is all the greater as the bending stiffness is low considering the possible slippage between the fibers. The objective of this section is to analyze the link between the onset and the development of wrinkles and the bending stiffness (and also tension and shear stiffnesses). The concept of a shear locking angle is also questioned.

The virtual work theorem (Eq. (2) and (3)) can be written, in any virtual displacement field $\boldsymbol{\eta}$ such as $\boldsymbol{\eta} = 0$ on the boundary with

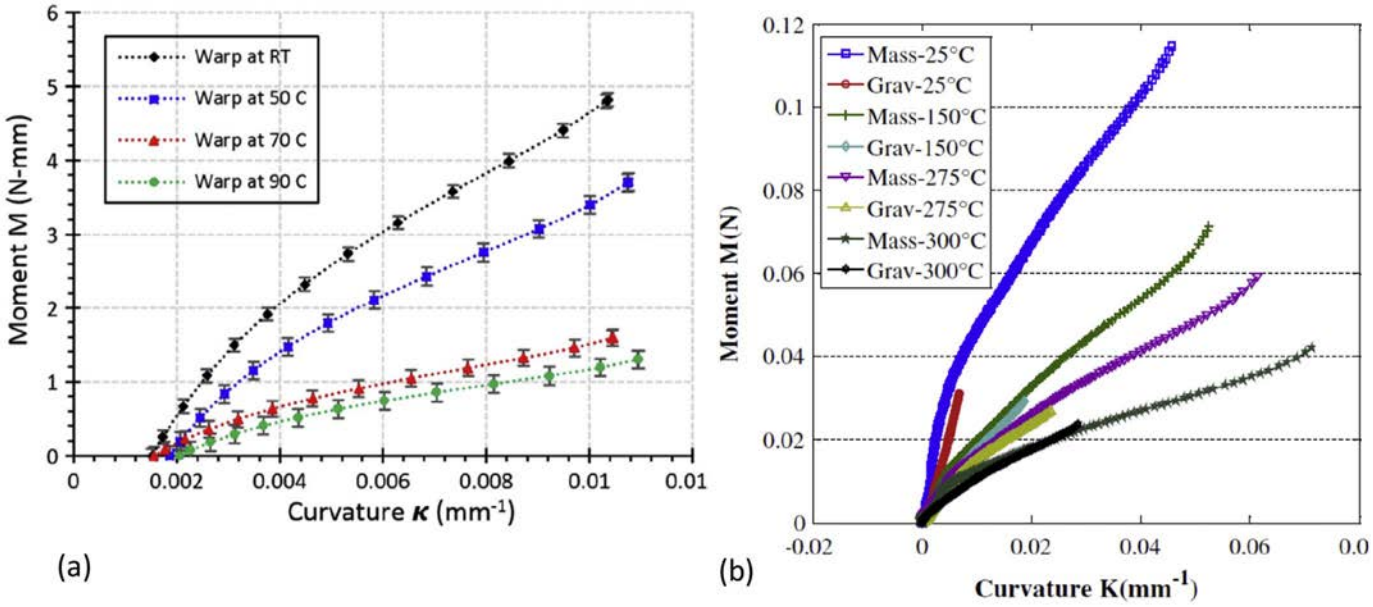

Fig. 13. Bending moment-Curvature curves for different temperatures. (a) 5-harness carbon satin and epoxy prepreg [69]. (b) 5-harness carbon satin and PPS prepreg [65].

prescribed displacements,

$$W_{ext}(\eta) - W_{int}^{tens}(\eta) - W_{int}^{shear}(\eta) - W_{int}^{bend}(\eta) = W_{acc}(\eta) \quad (12)$$

where $W_{int}^{tens}(\eta)$, $W_{int}^{shear}(\eta)$, $W_{int}^{bend}(\eta)$ are respectively the virtual works of tension, in-plane shear and bending. Wrinkles develop when the virtual work theorem leads to off-plan solutions. This is a global equation involving tension, in-plane shear and bending virtual works.

4.1. Wrinkling in compression in the yarn direction

When a textile reinforcement is subjected to a compression in the yarn direction, buckling occurs rapidly. The bending energy generated by the buckling is smaller than the compression energy that would be required by a compression deformation of the yarns. Fig. 14 shows the computed deformed shapes of an 80 × 20 mm textile strip whose two edges are moved closer (40 mm) [16]. The size of wrinkles that develop increases with bending stiffness. In this example (Fig. 14), when the bending stiffness is multiplied by ten, the number of wrinkles is divided by two. The fact that the size of the wrinkles depends on the bending stiffness has been observed in other cases. Nevertheless, it was also found to have a relatively low sensitivity to the bending stiffness [44,65]. There is, however, no consensus on this subject at present. Ropers et al. [73] state that a twofold difference in bending stiffness clearly modifies the result of a half-dome simulation forming.

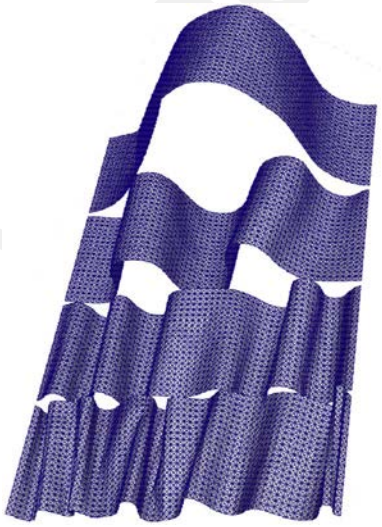

Fig. 14. Wrinkling in compression of a woven reinforcement strip with different bending stiffnesses (from bottom to top 1, 10, 10^2, 10^3 N /mm).

Wrinkling in longitudinal compression such as that presented in Fig. 14 is almost immediate if the fabric is free. Nevertheless, forming processes are designed to avoid these situations. On the other hand, forming on double-curved geometries requires shear deformations in the plane of the textile reinforcements which cannot be avoided. The next section focuses on wrinkles when forming a textile reinforcement on a hemisphere.

4.2. Influence of tensile, in-plane shear and bending stiffnesses on wrinkling during the forming of a double curved shape

A very unbalanced woven fabric, with a ratio between the tensile stiffness in warp and weft directions equal to 250, has been considered. The experiment shown in Fig. 15d was carried out in Nottingham University [108]. The simulation was performed by considering exclusively the tensile strain energy in Fig. 15a, the tensile and in-plane shear strain energies in Fig. 15b, and finally the three stain energies, i.e., tension, in plane shear and bending, in Fig 15c. Only the latter case led to a deformed shape in agreement with experimental results. The simulation based on the membrane hypothesis (no bending stiffness, Fig 15b) gave wrinkles that were small and plentiful. To obtain wrinkles of a correct geometry by the simulation, a bending stiffness is necessary. There is an important connection between wrinkles and bending stiffness and the latter determines their shape (and therefore their number).

Amirbayat and Hearle have analyzed textile fabric buckling through minimization of the deformation energy in three fold buckling which is the basic form for more complicated buckling patterns [109–111]. They showed that the deformed shape can be related to dimensionless groups, relating bending, membrane and potential energies, and fixed by sheet parameters [109,110,112].

4.3. Wrinkling and shear locking angle

The in-plane shear deformation required for forming on a double curved surface is one of the main causes of wrinkling. In-plane shear tests of textile reinforcements and in particular the 'picture frame test'

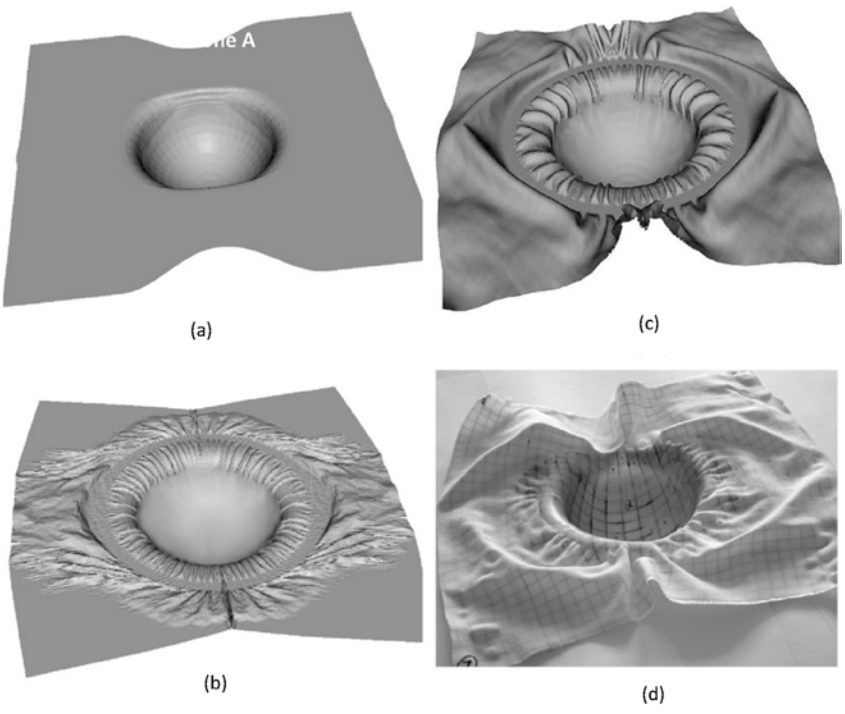

Fig. 15. Hemispherical forming of an unbalanced textile reinforcement, (a) tensile stiffness only, (b) tensile and in-plane shear rigidities, (c) tensile + in-plane shear + bending rigidities, (d) Experimental forming.

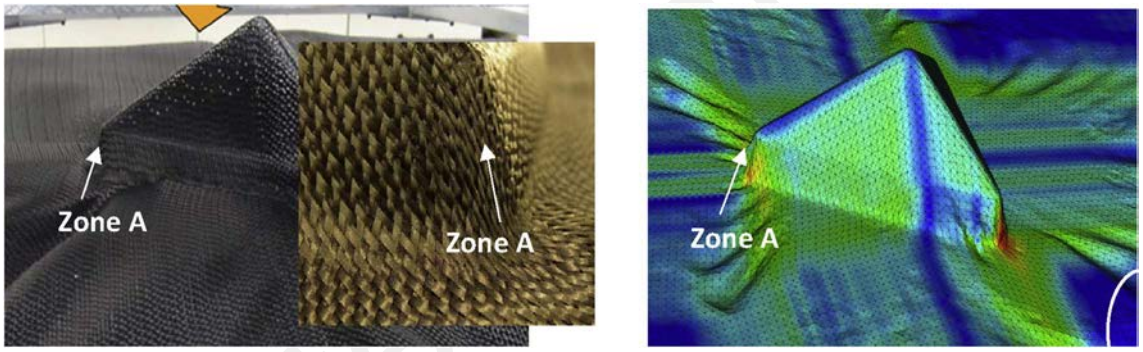

Fig. 16. A zone A with a shear angle of 60° (zone A) with no wrinkle. Some wrinkles develop in areas where the shear angles are less than 40°.

highlight an angle from which the wrinkling appears. This angle is called the 'shear locking angle' [113–117]. Some textile forming simulation approaches, and in particular a kinematic modeling approach, consider that wrinkling occurs when this angle is reached or exceeded. The example shown in Fig. 16 shows the opposite. This is the forming of a woven carbon reinforcement by a tetrahedric punch with several blank holders [46] (already shown in Fig. 4). In zone A, both experimentally and in simulation, the shear angle reaches 60° without any wrinkle onset. On the other hand, wrinkles develop in many other areas of the horizontal part of the reinforcement where the shear angle is less than 40°.

The wrinkle onset does not depend solely on the shear angle; the other strain energies also play a role. The deformations of the textile reinforcement and in particular the wrinkles are a solution of the global equation (12) (Virtual work theorem). The blank holders (which have an important effect in the case shown in Fig. 16) create tensions that decrease or suppress wrinkling in the useful part. Finally, the shear locking angle is not sufficient to determine the wrinkle onset. Wrinkles are given by the solution of the global dynamic equation (12) and all the deformation energies play a role [16,118–122].

4.4. Wrinkling of UD laminates during forming

The analyses regarding wrinkling presented above concern a single woven ply. Composites are often laminated and composed of a set of plies, and the actions between the plies are an important part of the development of wrinkles. This is particularly the case for laminates composed of unidirectional plies.

Composites with continuous unidirectional reinforcements (UD) are used in applications where stiffness is a major concern. The stiffness is optimal because the fibers are straight. The different plies of prepregs (or reinforcements) can be draped by hand or by an automated fiber placement [6,123]. Alternatively, a flat laminate made of UD plies can be formed into the final shape [50]. During the manufacture of composites from UD prepregs, the formation of wrinkling is frequent [124–126]. Such wrinkling can be severe (Fig. 17) [126–129]. Several studies have aimed to understand the causes of these wrinkles and how to avoid them [125–130].

Generally, wrinkling of a ply of a stack occurs when the ply is subjected to compressive stresses in the direction of its fibers. The UD plies are very anisotropic since the tensile rigidity is high in the direction of the fibers and almost zero in the perpendicular direction. Contact and friction create a connection between the plies. For a given geometry of the manufactured part, compressive stresses in the

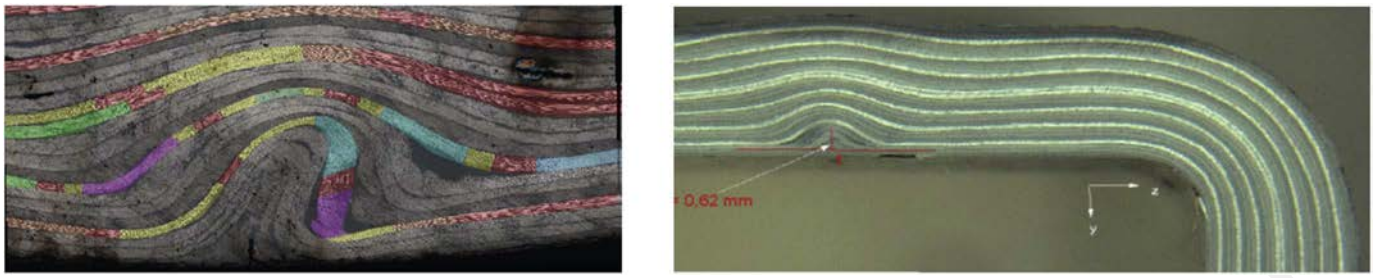

Fig. 17. Wrinkles induced by forming [126,127].

directions of the fibers (leading to wrinkles) can be applied on some plies for certain stacking sequences. Wrinkling can be reduced by changing the stacking sequence, however, this would modify the mechanical properties of the final composite.

Lightfoot et al. highlighted one of the main mechanisms of wrinkle formation during the prepreg stacking [127]. In a U-shaped mold, two plies at 90° and 0° were draped in this order. The first 90 °-ply correctly fit the U mold and its corner due to its low stiffness. On the contrary, the 0 °-ply was rigid in the direction of the fibers and the contact in the radius was not perfect during the draping on the mold (bridging ply). The autoclave pressure ensured the contact of the 0° ply in the radius. This led to a movement of the ply and, due to the friction with the 90° ply, this movement created a wrinkling of the ply [127].

5. 3D modeling of the bending of a textile reinforcement. The need for generalized continuum mechanics

5.1. The limit of standard continuum mechanics of Cauchy

3D finite element modeling of textile reinforcements makes it possible to simulate the deformation of reinforcements of great thickness and cases where the phenomena in the reinforcement thickness play an important role. Interlock reinforcement (such as that shown in Fig. 3) is used in motor blades with a thickness reaching several centimeters in the root of the fan blade [131–133]. These interlock materials consist of two yarn directions (warp and weft) that are linked in the thickness by weaving. Such an architecture makes it possible to avoid delamination. There is no yarn in the thickness direction. Among the hyperelastic models proposed for anisotropic materials [134,135], a constitutive law has been proposed in Ref. [80] for this type of interlock materials. The six deformation modes are considered (Fig. 18): extensions in the warp and weft directions (invariants I_{elong1} and I_{elong2}), in-plane shear (invariant I_{cp}) and transverse shear in the warp and weft directions (invariants I_{ct1} and I_{ct2}) and transverse compaction (invariant I_{comp}). The deformation energy is assumed to be the sum of deformation energies corresponding to the six deformation modes:

$$w = w_{elong1}(I_{elong1}) + w_{elong2}(I_{elong2}) + w_{comp}(I_{comp}) + w_{cp}(I_{cp}) + w_{ct1}(I_{ct1}) + w_{ct2}(I_{ct2}) \quad (13)$$

Appendix A gives the relations between the six above invariants and the theoretical invariants of a orthotropic material [136]. The six potential strain energies of Eq. (13) are identified from tension, transverse compression, in-plane shear and transverse shear tests [80,131].

A three-point bending of an interlock reinforcement was carried out experimentally and simulated using 3D hexahedral elements and the hyperelastic model presented above (Fig. 19a and b). The direction after deformation of the material lines initially perpendicular to the mid-surface of the interlock was fairly well obtained by the simulation. It was close to vertical. Nevertheless, in the simulation, the two outer parts remained almost horizontal (Fig. 19b) whereas experience shows that they should be rising (Fig. 19a). To understand this phenomenon, a simplified model was considered Fig. 19c [53]. The interlock specimen was modeled by a set of hinged parallel bar systems. The transverse shear stiffness of this 4 bar system was equal to zero (it was actually very weak in the textile reinforcement). When a vertical displacement was imposed at the center of the specimen, the deformation was simply due to the shear deformations in the part between the supports of the specimen (Fig. 19d). The deformed shape obtained for this simplified model was close to that obtained by the continuous 3D hyperelastic model (Fig. 19b), which implies that the two outer parts remained almost horizontal in this case. The shear stiffness of the textile reinforcement was very low because of the possible sliding between fibers and close to that of the bar system which was zero.

In the simplified model, if the bars were replaced by beams, an elevation of the ends was obtained (Fig. 19e). The flexural stiffness of the beams represented that of the fibers. Each fiber had a very small diameter and therefore a low bending rigidity, but the number of fibers was significant. It is not possible in a Cauchy mechanical model to simultaneously have a very low shear stiffness (because of the possible slippage between the fibers) and a bending stiffness originating from the fibers. This is the limit of Cauchy mechanical models in textile reinforcement deformation simulation.

The next two sections present possible approaches to correctly

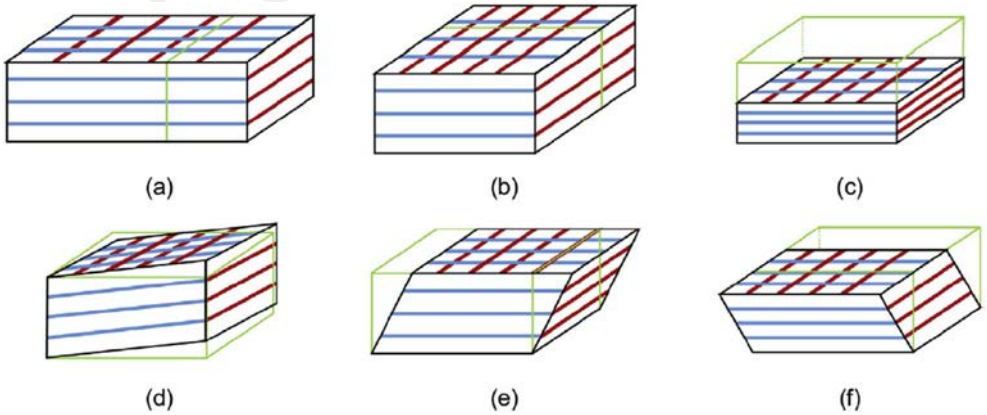

Fig. 18. Deformation modes of layer to layer interlock reinforcements (a and b) stretches, (c) transverse compression, (d) in-plane shear and (e and f) transverse shears.

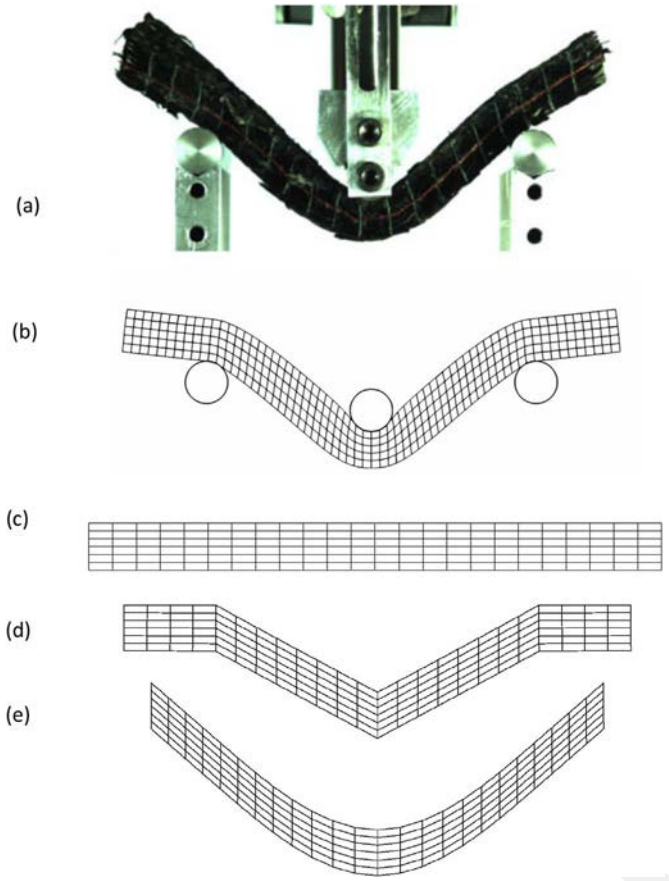

Fig. 19. Three point bending of an interlock reinforcement. (a) Experiment, (b) simulation based on a model of Cauchy, (c) hinged bar system: initial, (d) hinged bar system: deformed shape, (e) beams instead of bars.

model the bending of fibrous materials in the context of a 3D continuous approach. In section 5.1, a stiffness related to the curvature is added to the 3D hexahedral finite elements, and in section 5.2, a second gradient approach is used to take into account the local bending stiffness of the fibers.

5.2. 3D hexahedral finite elements with curvature stiffness

In rotation-free shell elements, the curvature of a finite element is calculated from the position of the neighboring elements without the need for rotational degrees of freedom [137,138]. This approach is extended to calculate the curvature of 3D hexahedral finite elements (Fig. 20a) [131,139]. Additional internal nodal loads are calculated from these curvatures. They reflect the local bending stiffness of the fibers. The kinematics (interpolation functions) of the element is not modified and is that of a classical trilinear 8 node finite element. Points fixed on the neighboring elements makes it possible to calculate the curvature. The approach is technically similar to those used in free rotation shell elements [137,138]. It is detailed in Ref. [131]. The curvature χ of the fibers creates a local bending moment $M(\chi)$. The internal virtual work corresponding to the virtual curvature χ^* is:

$$W_{\text{int}}^{bend} = \int_A M(\chi)\chi^* dA \tag{14}$$

In an 8 node finite element:

$$W_{\text{int}}^{bend} = \sum_{\alpha=1}^{2} \omega_\alpha M(\chi(\psi_\alpha))\ \chi^*(\psi_\alpha)\ A(\psi_\alpha)\ J_{s\alpha} \tag{15}$$

For two integration points ψ_α, $J_{s\alpha}$ is the jacobian of the mapping from the isoparametric domain of bi-unit length [-1,1] to the physical domain. The curvature interpolations can be written as:

$$\chi_{11} = B_1 u_p \qquad \text{and} \qquad \chi_{22} = B_2 u_p \tag{16}$$

where u_p is a vector containing the displacement of each node of the patch used to calculate the curvature. B_1 and B_2 are detailed in Ref. [131]. The bending moment in eqs. (14) and (15) is assumed to be dependent on the curvature $M = M(\chi)$. The nodal internal loads due to the local bending stiffness at each node of the patch of triangular elements can be computed as:

$$(F_{\text{int}}^{\text{bend}})_p = (B_1^T M_{l1} + B_2^T M_{l2})A_T \tag{17}$$

The simulation of the three-point bending test using these 3D finite elements with curvature stiffness led to a deformed shape in good agreement with experiments (Fig. 20b). Other simulations based on such enhanced 3D elements can be found in Refs. [131,139].

5.3. Second gradient approach

Models developed in the framework of the generalized continuum mechanics (in particular the second gradient models), bring improvements beyond the standard continuum mechanics of Cauchy [55,56,140–144]. To avoid the difficulties highlighted in section 5.1 in 3D simulations of textile reinforcement bending, a second gradient 3D orthotropic model can be introduced [54,145–149]. The strain energy density depends both on the right Cauchy-Green tensor **C** and on its gradient:

$$\mathrm{W}(\mathbf{C}, \nabla\mathbf{C}) = \mathrm{W_I}(\mathbf{C}) + \mathrm{W_{II}}(\nabla\mathbf{C}) \tag{18}$$

Here, $\mathrm{W_I}$ is the strain energy of the Cauchy model (first gradient) and $\mathrm{W_{II}}$ is the second gradient strain energy. It takes the local curvature of the continuum into account and consequently makes it possible to take into consideration the local fiber bending regardless of the first gradient behavior.

The second gradient energy introduced from the invariants defined in section 5.1 can be in the following form:

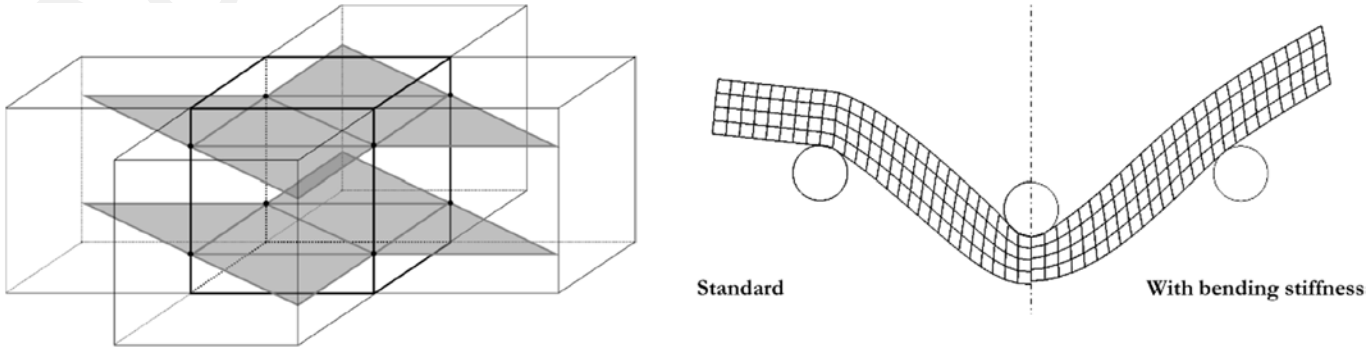

Fig. 20. (a) Computation of the curvature in a hexahedral element, (b) Improvement of the three point bending test simulation [131].

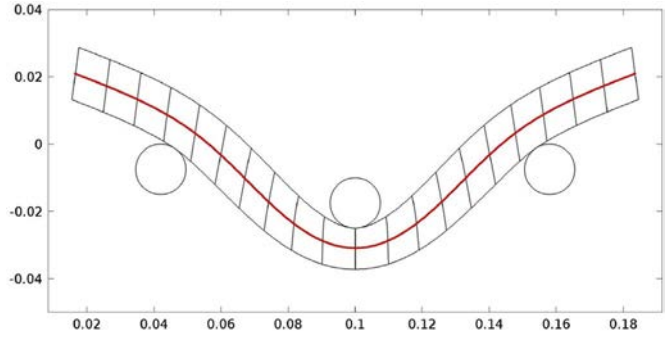

Fig. 21. Improvement of the 3 point bending test simulation by the use of a second gradient approach [54].

$$W_{II}(\nabla \mathbf{C}) = W_{II}(\nabla I_{cp}, \nabla I_{ct1}, \nabla I_{ct2}) = \frac{1}{2} ks_{cp} \|\nabla I_{cp}\|^2 + \frac{1}{2} ks_{ct1} \|\nabla I_{ct1}\|^2 + \frac{1}{2} ks_{ct2} \|\nabla I_{ct2}\|^2 \quad (19)$$

In this second gradient strain energy, the gradients of I_{ct1} and I_{ct2} are measures of the out-of-plane curvatures of the warp and weft fibers, respectively. The gradient of the invariant I_{cp} is associated with the in-plane bending of the fibers. As a consequence, the second gradient material parameters ks_{cp}, ks_{ct1} and ks_{ct2} represent the in-plane and out of plane bending stiffness of the fibres.

Different approaches are possible depending in particular on the internal architecture of the reinforcement and the stresses. In a general way, the terms of the second gradient relate to shear deformations that are major in the case of textile reinforcements since the fibers are almost inextensible [54,146]. The deformation obtained during the simulation of the three-point bending test using a second gradient model is presented in Fig. 21. It is in correct agreement with experiments. Second gradient models have shown to be of interest in different cases of forming and bending of textile composite reinforcements [150–152].

A comparison of the deformed midlines obtained experimentally and by the different approaches presented in sections 5 and 6 for the simulation of the three point bending of the thick interlock specimen (Fig. 19a)) is presented in Fig. 22. The deformed shaped obtained using the Cauchy model shows a too small radius of curvature at the center of the specimen and free extremities that do not rise enough. The other approaches are all close to the experiments.

6. Specific shell approaches for the bending of textile reinforcements

The possible slippage between the fibers of a textile reinforcement leads to a bending behavior that is not correctly described by the classical shell theories of Kirchhoff and Mindlin. In particular, the bending and membrane stiffnesses are not simply related by the thickness of the plate as this is the case for continuous materials in conventional theory. For textile reinforcements, it is possible to decouple the membrane deformation and bending energies as is done in Eqs. (2) and (3). The bending deformation energy is determined by the relation M(χ) (bending moment-curvature) which can be determined by the experimental methods presented in Section 3. A finite element analysis (or an analytical calculation in some cases) based on the behavior M(χ) makes it possible to determine the mid-surface of the deformed reinforcement (Figs. 4, 14 and 15c and 16). Nevertheless, the displacements and strains in the thickness are not specified. In some analyses, it is not necessary to have knowledge of them, whereas in other cases, and in particular for thick textile reinforcements, the material directions initially perpendicular to the mid-surface (so called 'normals') rotate in a very specific manner (e.g., Fig. 19a). The classical theories of plates provide displacements and strains in the thickness direction. They are irrelevant for fibrous reinforcements. Beyond the problem of non-coupling of the membrane and bending stiffnesses, Kirchhoff's theory assumes that material directions initially perpendicular to the surface remain perpendicular after deformation. The deformed shapes shown in Figs. 3, 9 and 19a, 23 and 24 for example clearly demonstrate that the bending behavior of the textile reinforcement is far from Kirchhoff's theory.

In Mindlin's theory, the curvature is the derivative of the rotation of the normal (material direction initially perpendicular to the mid-surface). This is not the case for fibrous reinforcements. For example, as can be seen in Fig. 23, between sections 1 and 3, the normals remained vertical but the curvature was non-zero. Moreover, trying to simulate the bending of a textile reinforcement using Mindlin shell finite elements did not give a result in agreement with experiments [57].

The physics of textile reinforcement bending is specific. It is based on the quasi-inextensibility of the fibers on the one hand and on the possibility of sliding between the fibers on the other hand. Liang et al. proposed a shell finite element for textile composite reinforcements based on Ahmad's approach [57,153]. The finite element is shown in Fig. 23c. It consists of parallel fibers, and the internal virtual work of the element is obtained as the sum of virtual works of tension and of the

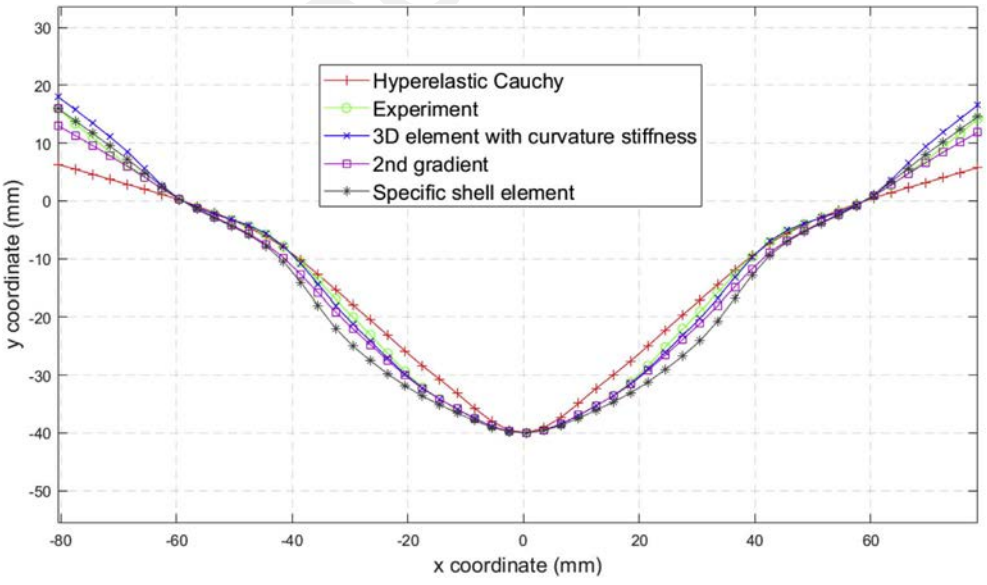

Fig. 22. Comparison of the deformed midline obtained for the 3 point bending of the interlock specimen for the different approaches presented in section 5 and 6.

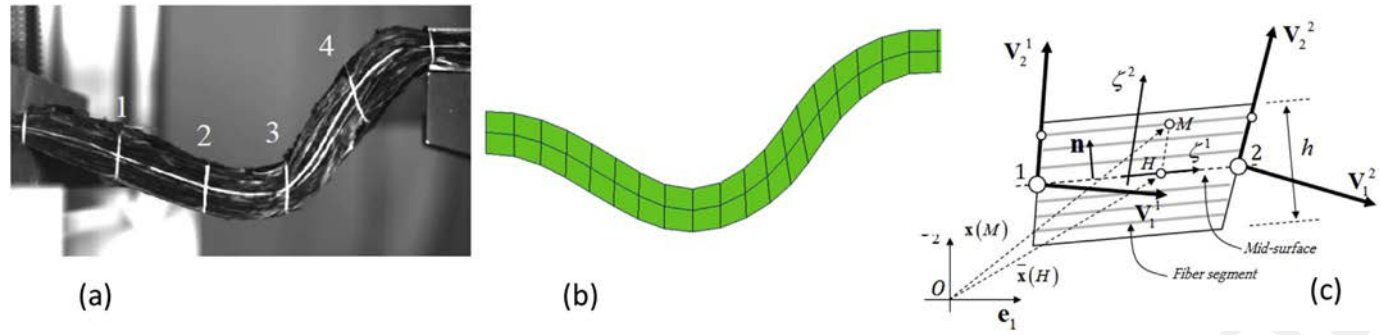

Fig. 23. Bending test on a multilayer reinforcement: (a) Experiment. (b) Simulation (c) Ahmad shell finite element.

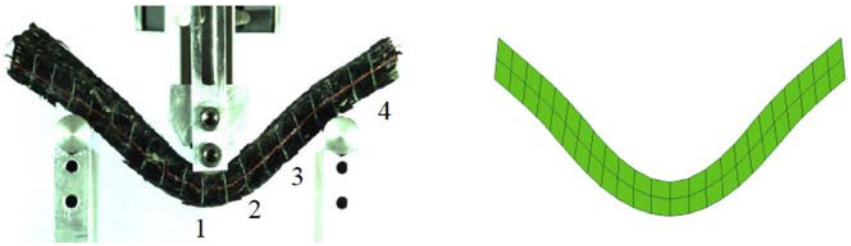

Fig. 24. Three points bending tests on an interlock reinforcement: Left: experiment, right: simulation [57].

bending of each fiber.

$$\delta W_{\text{int}}^{e} = \sum_{f=1}^{n} \int_{L^f} T^{11f} \delta\varepsilon_{11}{}^{f} dL + \sum_{f=1}^{n} \int_{L^f} M^{33f} \delta\chi_{33}{}^{f} dL \tag{20}$$

Here, T^{11} and M^{33} are the tension load and bending moment on the fiber segment f, respectively, and $\delta\varepsilon_{11}$ and $\delta\chi_{33}$ are respectively the virtual tensile strain and curvature. The tensile and bending strains can be calculated precisely using neighboring elements. This specific shell element gives results that are in good agreement with experiment, especially in terms of rotations of the normals (Fig. 23). The simulation of the three-point bending of the interlock reinforcement studied in Section 5 is shown in Fig. 24. The results are accurate using a very low number of degrees of freedom (20 dof in Fig. 24). Friction between fibers plays a major role in the bending stiffness. It can be taken into account in the bending stiffness of each fiber. Other simulations and comparisons with experiments are presented in Ref. [57]. Sheet metal forming simulations are made using shell finite elements based on Kirchhoff or Mindlin theories (classical). A specific shell theory (non-classical) should be necessary for fibrous reinforcements. Much remains to be done and in particular this approach should be extended to 3D shells.

7. Conclusion

Modeling and draping simulation of composite reinforcements represent a very active area of research. Although the first simulations of textile reinforcement forming were carried out under the hypothesis of a membrane, it has been shown that the bending stiffness, although weak, played a significant role: in particular, it determines the size of the wrinkles. The physics of bending are not the same for a continuous plate, made for instance of metal, and for a textile reinforcement. In the first case, the bending corresponds to an extension strain on one side of the mid-surface and to a compressive strain on the other side. In the case of fibrous reinforcements, the fibers are almost inextensible, but there are slippages between the fibers that create bending.

Many experimental works have been carried out to measure flexure of fibrous materials. Three main test families have been developed: cantilever bending, Kawabata test (imposed curvature), and three-point bending. Extensions of these tests at different temperatures and at different speeds are currently developed. Their objective is to identify thermomechanical and viscoelastic flexural models (especially for prepregs). Although the first tests, and in particular Peirce's test, are almost a century old, the development of these experimental methods is very active today.

Bending of fibrous reinforcements is not correctly modeled by standard bending theories. What is needed is a theory for the bending of fibrous reinforcements which would be for fibrous reinforcements what the Kirchhoff and Mindlin models are for sheet metal. In the case of 3D modeling it has been shown that standard Cauchy models cannot correctly describe the local bending stiffness of fibers. Generalized continuum mechanics models that are sufficiently simple and effective for the simulation of the forming of textile reinforcements thus need to be developed.

Appendix A

For an orthotropic material, the strain energy density function of a hyperelastic law is of the form [136]:

$$w^{orth} = w^{orth}(I_1, I_2, I_3, I_{41}, I_{42}, I_{43}, I_{412}, I_{423}, I_{51}, I_{52}, I_{53}) \tag{A.1}$$

where I_1, I_2, I_3, are the invariants of the right Cauchy-green tensor $\underline{\underline{C}}$ defined by:

$$\begin{aligned} I_1 &= Tr(\underline{\underline{C}}) \\ I_2 &= \tfrac{1}{2}(Tr(\underline{\underline{C}})^2 - Tr(\underline{\underline{C}}^2)) \\ I_3 &= Det(\underline{\underline{C}}) \end{aligned} \tag{A.2}$$

and the mixed invariants (i and j = 1,3):

$$I_{4i} = \underline{\underline{C}} : \underline{\underline{M}}_i = \underline{M}_i \cdot \underline{\underline{C}} \cdot \underline{M}_i,$$
$$I_{4ij} = \underline{M}_i \cdot \underline{\underline{C}} \cdot \underline{M}_j,$$
$$I_{5i} = \underline{\underline{C}}^2 : \underline{\underline{M}}_i = \underline{M}_i \cdot \underline{\underline{C}}^2 \cdot \underline{M}_i \quad \text{(A.3)}$$

$\underline{M}_1$, $\underline{M}_2$ are the warp and weft directions and $\underline{M}_3$ is perpendicular to them. The structural tensors are defined for a material based on such $\underline{M}_i$ vectors (i ranges from 1 to 3):

$$\underline{\underline{M}}_1 = \underline{M}_1 \otimes \underline{M}_1,$$
$$\underline{\underline{M}}_2 = \underline{M}_2 \otimes \underline{M}_2$$
$$\text{and} \quad \underline{\underline{M}}_3 = \underline{M}_3 \otimes \underline{M}_3 \quad \text{(A.4)}$$

The six strain invariants of the right Cauchy-Green tensor **C**, based on physical observations I_{elong1}, I_{elong2}, I_{comp}, I_{cp}, I_{ct1}, I_{ct2} and are function of the invariants defined in Eqs. (A.2) and (A.3).

$$I_{elong1} = \frac{1}{2} ln(I_{41})$$
$$I_{elong2} = \frac{1}{2} ln(I_{42})$$
$$I_{comp} = \frac{1}{2} ln\left(\frac{I_3}{I_{41} I_{42} (1 - I_{cp}^2)}\right) \quad \text{(A.5)}$$

$$I_{cp} = \frac{I_{412}}{\sqrt{I_{41} I_{42}}} \quad I_{ct1} = \frac{I_{413}}{\sqrt{I_{41} I_{43}}} \quad I_{ct2} = \frac{I_{423}}{\sqrt{I_{42} I_{43}}} \quad \text{(A.6)}$$

The six strain energies of the hyperelastic model have been identified from tensile tests in the warp and weft directions, compaction test, bias extension test (in-plane shear), and simple transverse shear tests. The corresponding identifications are detailed in Refs. [80,131].

References

[1] Weimer C. The future composite materials challenge in aeronautics. ECCM 17 conference, Munich. 2016.
[2] Meola C, Boccardi S. Composite materials in the aeronautical industry. Infrared Thermography to Composites. Woodhead; 2017. p. 1–24.
[3] Friedrich K, Almajid AA. Manufacturing aspects of advanced polymer composites for automotive applications. Appl Compos Mater 2013;20(2):107–28.
[4] Ruiz E, Trochu F. Flow modeling in composite reinforcements. Compos Reinforcements for Optimum Perform 2011:588–615.
[5] Sozer E, Simacek P, Advani S. Resin transfer molding (RTM) in polymer matrix composites. Manuf Tech Polym Matrix Compos 2012:245–309.
[6] Lukaszewicz D, Ward C, Potter KD. The engineering aspects of automated prepreg layup: history, present and future. Compos B Eng 2012;43(3):997–1009.
[7] Lukaszewicz D, Potter KD, Eales J. A concept for the in situ consolidation of thermoset matrix prepreg during automated lay-up. Compos B Eng 2013;45(1):538–43.
[8] Qureshi Z, Swait T, Scaife R, El-Dessouky HM. In situ consolidation of thermoplastic prepreg tape using automated tape placement technology: potential and possibilities. Compos B Eng 2014;66:255–67.
[9] Prabhu VA, Elkington M, Crowley D, Tiwari A, Ward C. Digitisation of manual composite layup task knowledge using gaming technology. Compos B Eng 2017;112:314–26.
[10] Cherouat A, Billoët JL. Mechanical and numerical modelling of composite manufacturing processes deep-drawing and laying-up of thin pre-impregnated woven fabrics. J Mater Process Technol 2001;118(1–3):460–71.
[11] Lin H, Wang J, Long AC, Clifford MJ, Harrison P. Predictive modelling for optimization of textile composite forming. Compos Sci Technol 2007;67:3242–52.
[12] Lee J, Hong S, Yu W, Kang T. The effect of blank holder force on the stampforming behaviour of non-crimp fabric with a chain stitch. Compos Sci Technol 2007;67(3–4):357–66.
[13] Ten Thije RHW, Akkerman R, Huetink J. Large deformation simulation of anisotropic material using an updated Lagrangian finite element method. Comput Meth Appl Mech Eng 2007;196(33–34):3141–50.
[14] Skordos AA, Aceves CM, Sutcliffe MPF. A simplified rate dependent model of forming and wrinkling of pre-impregnated woven composites. Compos Part A 2007;38:1318–30.
[15] Chen S, Harper LT, Endruweit A, Warrior NA. Formability optimisation of fabric preforms by controlling material draw-in through in-plane constraints. Compos A Appl Sci Manuf 2015;76:10–9.
[16] Boisse P, Hamila N, Vidal-Sallé E, Dumont F. Simulation of wrinkling during textile composite reinforcement forming. Influence of tensile, in-plane shear and bending stiffnesses. Compos Sci Technol 2011;71(5):683–92.
[17] Sjölander J, Hallander P, Åkermo M. Forming induced wrinkling of composite laminates: a numerical study on wrinkling mechanisms. Compos A Appl Sci Manuf 2016;81:41–51.
[18] Harrison P. Modelling the forming mechanics of engineering fabrics using a mutually constrained pantographic beam and membrane mesh. Compos A Appl Sci Manuf 2016;81:145–57.
[19] Kawabata S, Niwa M, Kawai H. The finite deformation theory of plain weave fabrics. Part I: the biaxial deformation theory. J Textil Inst 1973;64(1):21–46.
[20] Buet-Gautier K, Boisse P. Experimental analysis and modeling of biaxial mechanical behavior of woven composite reinforcements. Exp Mech 2001;41(3):260–9.
[21] Carvelli V, Corazza C, Poggi C. Mechanical modelling of monofilament technical textiles. Comput Mater Sci 2008;42:679–91.
[22] Willems A, Lomov SV, Verpoest I, Vandepitte D. Optical strain fields in shear and tensile testing of textile reinforcements. Compos Sci Technol 2008;68:807–19.
[23] Skelton J. Fundamental of fabric shear. Textil Res J 1976;46(12):862–9.
[24] Wang J, Page JR, Paton R. Experimental investigation of the draping properties of reinforcement fabrics. Compos Sci Technol 1998;58:229–37.
[25] Potter K. Bias-extension measurements on cross-plied unidirectional prepreg. Compos Part A 2002;33:63–73.
[26] Zouari B, Daniel JL, Boisse P. A woven reinforcement forming simulation method. Influence of the shear stiffness. Comput Struct 2006;84(5):351–63.
[27] Cao J, Akkerman R, Boisse P, Chen J, Cheng HS, de Graaf EF, et al. Characterization of mechanical behavior of woven fabrics: experimental methods and benchmark results. Compos Part A 2008;39:1037–53.
[28] Boisse P, Hamila N, Guzman-Maldonado E, Madeo A, Hivet G, Dell'Isola F. The bias-extension test for the analysis of in-plane shear properties of textile composite reinforcements and prepregs: a review. Int J Material Form 2017;10(4):473–92.
[29] Peirce FT. The "handle" of cloth as a measurable quantity. J Textil Inst Trans 1930;21(9):T377–416.
[30] Peirce FT. The geometry of cloth structure. J Textil Inst Trans 1937;28(3):T45–96.
[31] ASTM. Standard test method for stiffness of fabrics, chap. D1388–D1396(2002). Philadelphia: American Society for Testing and Materials; 2002.
[32] ISO. Reinforcement fabrics — determination of conventional flexural stiffness — fixed-angle flexometer method ISO 4604. 2011.
[33] British Standard. Textiles—test methods for nonwovens—Part 7: determination of bending length, BS EN ISO 9073–9077. 1998.
[34] Kawabata S. The standardization and analysis of hand evaluation. Osaka: The Textile Machinery Society of Japan; 1980.
[35] Grosberg P. The mechanical properties of woven fabrics part ii: the bending of woven fabrics. Textil Res J 1966;36(3):205–14.
[36] Dahl P. Solid friction damping of mechanical vibrations. AIAA J 1976;14(12):1675–82.
[37] Syerko E, Comas-Cardona S, Binetruy C. Models of mechanical properties/behavior of dry fibrous materials at various scales in bending and tension: a review. Compos A Appl Sci Manuf 2012;43(8):1365–88.
[38] Bliman P, Sorine M. Easy-to-use realistic dry friction models for automatic control. 3rd European control conference, Rome, Italy. 1995. p. 3788–94.
[39] Lahey T, Heppler G. Mechanical modeling of fabrics in bending. J Appl Mech 2004;71:32–40.
[40] Bliman PA, Sorine M. Friction modeling by hysteresis operators. Application to Dahl, sticktion and Stribeck effects. London: Longman Scientific and Technical; 1993.
[41] Timoshenko SP, Woinowsky-Krieger S. Theory of plates and shells. McGraw-Hill; 1959.
[42] Dhatt G, Batoz JL. Modélisation des structures par éléments finis: poutres et plaques. Presses de l'Université Laval; 1990.
[43] Zienkiewicz OC, Taylor RL. The finite element method for solid and structural mechanics. Butterworth-Heinemann; 2005.
[44] Hamila N, Boisse P, Sabourin F, Brunet M. A semi-discrete shell finite element for textile composite reinforcement forming simulation. Int J Numer Meth Eng 2009;79(12):1443–66.

[45] Jauffrès D, Sherwood JA, Morris CD, Chen J. Discrete mesoscopic modeling for the simulation of woven-fabric reinforcement forming. Int J Material Form 2010;3(2):1205–16.
[46] Allaoui S, Boisse P, Chatel S, Hamila N, Hivet G, Soulat D, et al. Experimental and numerical analyses of textile reinforcement forming of a tetrahedral shape. Compos A Appl Sci Manuf 2011;42(6):612–22.
[47] Bel S, Hamila N, Boisse P, Dumont F. Finite element model for NCF composite reinforcement preforming: importance of inter-ply sliding. Compos A Appl Sci Manuf 2012;43(12):2269–77.
[48] Gereke T, Döbrich O, Hübner M, Cherif C. Experimental and computational composite textile reinforcement forming: a review. Composites 2013;46:1–10.
[49] Margossian A, Bel S, Balvers JM, Leutz D, Freitas R, Hinterhoelzl R. Finite element forming simulation of locally stitched non-crimp fabrics. Compos A Appl Sci Manuf 2014;61:152–62.
[50] Leutz D, Vermilyea M, Bel S, Hinterhölzl R. Forming simulation of thick afp laminates and comparison with live CT imaging. Appl Compos Mater 2016;23(4):583–600.
[51] Hübner M, Rocher JE, Allaoui S, Hivet G, Gereke T, Cherif C. Simulation-based investigations on the drape behavior of 3D woven fabrics made of commingled yarns. Int J Material Form 2016;9(5):591–9. On line.
[52] Schirmaier FJ, Dörr D, Henning F, Kärger L. A macroscopic approach to simulate the forming behaviour of stitched unidirectional non-crimp fabrics (UD-NCF). Compos A Appl Sci Manuf 2017;102:322–35.
[53] Boisse P, Hamila N, Madeo A. The difficulties in modeling the mechanical behavior of textile composite reinforcements with standard continuum mechanics of Cauchy. Some possible remedies. Int J Solid Struct 2016. On Line https://doi.org/10.1016/j.ijsolstr.2016.12.019.
[54] Madeo A, Ferretti M, Dell'Isola F, Boisse P. Thick fibrous composite re- inforcements behave as special second-gradient materials: three-point bend- ing of 3D interlocks. Z Angew Math Phys 2015;66(4):2041–60.
[55] Maugin GA. Generalized continuum mechanics: what do we mean by that? Mech Gen Contin 2010:3–13.
[56] Forest S. Micromorphic approach for gradient elasticity, viscoplasticity, and damage. J Eng Mech 2009;135(3):117–31.
[57] Liang B, Colmars J, Boisse P. A shell formulation for fibrous reinforcement forming simulations. Compos A Appl Sci Manuf 2017;100:81–96.
[58] Komeili M, Milani AS. On effect of shear-tension coupling in forming simulation of woven fabric reinforcements. Compos B Eng 2016;99:17–29.
[59] Van Der Ween F. Algorithms for draping fabrics on doubly curved surfaces. Int J Numer Meth Eng 1991;31:1414–26.
[60] Long AC, Rudd CD. A simulation of reinforcement deformation during the production of preform for liquid moulding processes. IMechE J Eng Manuf 1994;208:269–78.
[61] Potluri P, Sharma S, Ramgulam R. Comprehensive drape modelling for moulding 3D textile preforms. Compos Part A 2001;32(10):1415–24.
[62] Döbrich O, Gereke T, Diestel O, Krzywinski S, Cherif C. Decoupling the bending behavior and the membrane properties of finite shell elements for a correct description of the mechanical behavior of textiles with a laminate formulation. J Ind Textil 2014;44(1):70–84.
[63] Lammens N, Kersemans M, Luyckx G, Van Paepegem W, Degrieck J. Improved accuracy in the determination of flexural rigidity of textile fabrics by the Peirce cantilever test (ASTM D1388). Textil Res J 2014;84(12):1307–14.
[64] De Bilbao E, Soulat D, Hivet G, Gasser A. Experimental study of bending behaviour of reinforcements. Exp Mech 2010;50(3):333–51.
[65] Liang B, Hamila N, Peillon M, Boisse P. Analysis of thermoplastic prepreg bending stiffness during manufacturing and of its influence on wrinkling simulations. Compos Part A: Appl Sci Manuf 2014;67:111–22.
[66] Liang B, Chaudet P, Boisse P. Curvature determination in the bending test of continuous fibre reinforcements. Strain 2017;53(1).
[67] Dangora LM, Mitchell CJ, Sherwood JA. Predictive model for the detection of out-of-plane defects formed during textile-composite manufacture. Compos A Appl Sci Manuf 2015;78:102–12.
[68] Dangora LM, Mitchell C, White KD, Sherwood JA, Parker JC. Characterization of temperature-dependent tensile and flexural rigidities of a cross-ply thermoplastic lamina with implementation into a forming model. Int J Material Form 2016. On line https://doi.org/10.1007/s12289-016-1327-2.
[69] Alshahrani H, Hojjati M. A new test method for the characterization of the bending behavior of textile prepregs. Compos A Appl Sci Manuf 2017;97:128–40.
[70] Alshahrani H, Hojjati M. Bending behavior of multilayered textile composite prepregs: experiment and finite element modeling. Mater Des 2017;124:211–24.
[71] Sachs U, Akkerman R. Viscoelastic bending model for continuous fiber-reinforced thermoplastic composites in melt. Compos A Appl Sci Manuf 2017;100:333–41.
[72] Lomov SV, Verpoest I, Barburski M, Laperre J. Carbon composites based on multiaxial multiply stitched preforms. Part 2. KES-F characterisation of the deformability of the preforms at low loads. Compos A Appl Sci Manuf 2003;34(4):359–70.
[73] Ropers S, Kardos M, Osswald TA. A thermo-viscoelastic approach for the characterization and modeling of the bending behavior of thermoplastic composites. Compos A Appl Sci Manuf 2016;90:22–32.
[74] Yu J, Wang E, Li J, Zheng Z. Static and low-velocity impact behavior of sandwich beams with closed-cell aluminum-foam core in three-point bending. Int J Impact Eng 2008;35(8):885–94.
[75] Liu C, Du D, Li H, Hu Y, Xu Y, Tian J, et al. Interlaminar failure behavior of GLARE laminates under short-beam three-point-bending load. Compos B Eng 2016;97:361–7.
[76] Liu Q, Xu X, Ma J, Wang J, Shi Y, Hui D. Lateral crushing and bending responses of CFRP square tube filled with aluminum honeycomb. Compos B Eng 2017;118:104–15.
[77] Mitchell C, Dangora L, Bielmeier C, Sherwood J. Investigation into the changes in bending stiffness of a textile reinforced composite due to in-plane fabric shear: Part 1–Experiment. Compos A Appl Sci Manuf 2016;85:94–102.
[78] Caliskan U, Apalak MK. Low velocity bending impact behavior of foam core sandwich beams: Experimental. Compos B Eng 2017;112:158–75.
[79] Martin TA, Bennison SJ, Dykes RJ, Bhattacharyya D. Bending of continuous fibre-reinforced thermoplastic sheets. In: Bhattacharyya D, editor. Composite sheet forming of composite materials series. vol. 11. Elsevier; 1997. p. p.371–401.
[80] Charmetant A, Orliac JG, Vidal-Sallé E, Boisse P. Hyperelastic model for large deformation analyses of 3D interlock composite preforms. Compos Sci Technol 2012;72(12):1352–60.
[81] Margossian A, Bel S, Hinterhoelzl R. Bending characterisation of a molten unidirectional carbon fibre reinforced thermoplastic composite using a Dynamic Mechanical Analysis system. Compos A Appl Sci Manuf 2015;77:154–63.
[82] Martin TA, Bhattacharyya D, Collins IF. Bending of fibre-reinforced thermoplastic sheets. Compos Manuf 1995;6(34):177–87.
[83] Gangloff JJ, Simacek P, Sinha S, Advani SG. A process model for the compaction and saturation of partially impregnated thermoset prepreg tapes. Compos A Appl Sci Manuf 2014;64:234–44.
[84] Alshahrani H, Hojjati M. Experimental and numerical investigations on formability of out-of-autoclave thermoset prepreg using a double diaphragm process. Compos A Appl Sci Manuf 2017;101:199–214.
[85] Soulat D, Cheruet A, Boisse P. Simulation of continuous fibre reinforced thermoplastic forming using a shell finite element with transverse stress. Comput Struct 2006;84:888–903.
[86] Willems A, Lomov SV, Verpoest I, Vandepitte D, Harrison P, Yu WR. Forming simulation of a thermoplastic commingled woven textile on a double dome. Int J Material Form 2008;1:965–8.
[87] Wang P, Hamila N, Boisse P. Thermoforming simulation of multilayer composites with continuous fibres and thermoplastic matrix. Compos B Eng 2013;52:127–36.
[88] Harrison P, Gomes R, Curado-Correia N. Press forming a 0/90 cross-ply advanced thermoplastic composite using the double-dome benchmark geometry. Compos Part A 2013;54:56–69.
[89] Haanappel SP, Ten Thije RHW, Sachs U, Rietman B, Akkerman R. Formability analyses of uni-directional and textile reinforced thermoplastics. Compos A Appl Sci Manuf 2014;56:80–92.
[90] Guzman-Maldonado E, Hamila N, Boisse P, Bikard J. Thermomechanical analysis, modelling and simulation of the forming of pre-impregnated thermoplastics composites. Compos A Appl Sci Manuf 2015;78:211–22.
[91] Dörr D, Schirmaier FJ, Henning F, Kärger L. A viscoelastic approach for modeling bending behavior in finite element forming simulation of continuously fiber reinforced composites. Compos A Appl Sci Manuf 2017;94:113–23.
[92] Ropers S, Sachs U, Kardos M, Osswald TA. A thermo-viscoelastic approach for the characterization and modeling of the bending behavior of thermoplastic composites–Part II. Compos A Appl Sci Manuf 2017;96:67–76.
[93] Guzman-Maldonado E, Hamila N, Naouar N, Moulin G, Boisse P. Simulation of thermoplastic prepreg thermoforming based on a visco-hyperelastic model and a thermal homogenization. Mater Des 2016;93:431–42.
[94] Jayasree NA, Airale AG, Ferraris A, Messana A, Sisca L, Carello M. Process analysis for structural optimisation of thermoplastic composite component using the building block approach. Compos B Eng 2017;126:119–32.
[95] Dedieu C, Barasinski A, Chinesta F, Dupillier JM. About the origins of residual stresses in in situ consolidated thermoplastic composite rings. Int J Material Form 2017;10(5):779–92.
[96] Wang J, Long AC, Clifford MJ. Experimental measurement and predictive modelling of bending behaviour for viscous unidirectional composite materials. Int J Material Form 2010;3(2):1253–66.
[97] Alshahrani H, Hojjati M. A theoretical model with experimental verification for bending stiffness of thermosetting prepreg during forming process. Compos Struct 2017;166:136–45.
[98] Ghosh TK, Batra SK, Barker RL. The bending behaviour of plain-woven assemblies. Part I. A critical review. J Textil Inst 1990;81(3):245–54.
[99] Ghosh TK, Batra SK, Barker RL. The bending behaviour of plain-woven assemblies. Part II. The case of linear thread-bending behaviour. J Textil Inst 1990;81(3):272–87.
[100] Ghosh TK, Batra SK, Barker RL. The bending behaviour of plain-woven assemblies. Part III. The case of bilinear thread-bending behaviour and the effect of fabric set. J Textil Inst 1990;81(3):272–87.
[101] Lomov SV, Truevtzev AV, Cassidy C. A predictive model for the fabric-to-yarn bending stiffness ratio of a plain-woven set fabric. Textil Res J 2000;70(12):1088–96.
[102] Sagar TV, Potluri P. Computation of bending behavior of woven structures using optimization techniques. Textil Res J 2004;74(10):879–86.
[103] Hill R. A general theory of uniqueness and stability in elastic–plastic solids. J Mech Phys Solid 1958;8:236–49.
[104] Cao J, Boyce M. Wrinkle behavior of rectangular plates under lateral constraint. Int J Solid Struct 1997;34(2):153–76.
[105] Friedl N, Rammerstorfer FG, Fischer FD. Buckling of stretched strips. Comput Struct 2000;78(1–3):185–90.
[106] Lu H, Liu Y, Huang WM, Wang C, Hui D, Fu YQ. Controlled evolution of surface patterns for ZnO coated on stretched PMMA upon thermal and solvent treatments. Compos B Eng 2018;132:1–9.
[107] Mozafari H, Lin S, Tsui GC, Gu L. Controllable energy absorption of double sided corrugated tubes under axial crushing. Compos B Eng 2018;134:9–17.
[108] Daniel JL, Soulat D, Dumont F, Zouari B, Boisse P, Long AC. Forming simulation of

very unbalanced woven composite reinforcements. Int J Form Process 2003;6(3–4):465–80.
[109] Amirbayat J, Hearle JWS. The complex buckling of flexible sheet materials. Part I: theoretical approach. Int J Mech Sci 1986;28(6):339–58.
[110] Amirbayat J, Hearle JWS. The complex buckling of flexible sheet materials. Part II: experimental study of 3-fold buckling. Int J Mech Sci 1986;28(6):359–70.
[111] Amirbayat J, Hearle JWS. The anatomy of buckling of textile fabrics: drape and conformability. J Textil Inst 1989;80(1):51–69.
[112] Hearle JWS, Amirbayat J. Analysis of drape by means of dimensionless groups. Textil Res J 1986;56(12):727–33.
[113] Prodromou AG, Chen J. On the relationship between shear angle and wrinkling of textile composite preforms. Compos Part A 1997;28A:491–503.
[114] Lebrun G, Bureau MN, Denault J. Evaluation of bias-extension and pictureframe test for the measurement of shear properties of PP/glass commingled fabrics. Compos Struct 2003;61:52–341.
[115] Sharma SB, Sutcliffe MPF, Chang SH. Characterisation of material properties for draping of dry woven composite material. Compos Part A 2003;34:1167–75.
[116] Zhu B, Yu TX, Teng J, Tao XM. Theoretical modeling of large shear deformation and wrinkling of plain woven composite. J Compos Mater 2009;43(2):125–38.
[117] Hosseini A, Kashani MH, Sassani F, Milani AS, Ko FK. Identifying the distinct shear wrinkling behavior of woven composite preforms under bias extension and picture frame tests. Compos Struct 2017;185:764–73.
[118] Harrison P, Abdiwi F, Guo Z, Potluri P, Yu WR. Characterising the shear–tension coupling and wrinkling behaviour of woven engineering fabrics. Compos A Appl Sci Manuf 2012;43(6):903–14.
[119] Tullu A, Ku TW, Kang BS. Theoretical and numerical predictions of stretch-bending deformation behavior in composite sheet. Compos B Eng 2016;85:343–54.
[120] Arnold SE, Sutcliffe MPF, Oram WLA. Experimental measurement of wrinkle formation during draping of non-crimp fabric. Compos A Appl Sci Manuf 2016;82:159–69.
[121] Omrani F, Wang P, Soulat D, Ferreira M, Ouagne P. Analysis of the deformability of flax-fibre nonwoven fabrics during manufacturing. Compos B Eng 2017;116:471–85.
[122] Bardl G, Nocke A, Hübner M, Gereke T, Pooch M, Schulze M, et al. Analysis of the 3D draping behavior of carbon fiber non-crimp fabrics with eddy current technique. Compos B Eng 2018;132:49–60.
[123] Campbell FC. Manufacturing processes for advanced composites. Oxford: Elsevier Advanced Technology; 2004.
[124] Dodwell TJ, Butler R, Hunt GW. Out-of-plane ply wrinkling defects during consolidation over an external radius. Compos Sci Technol 2014;105:151–9.
[125] Haanappel SP, Ten Thije RHW, Sachs U, Rietman B, Akkerman R. Formability analyses of uni-directional and textile reinforced thermoplastics. Compos A Appl Sci Manuf 2014;56:80–92.
[126] Hallander P, Sjölander J, Åkermo M. Forming induced wrinkling of composite laminates with mixed ply material properties; an experimental study. Compos A Appl Sci Manuf 2015;78:234–45.
[127] Lightfoot JS, Wisnom MR, Potter K. A new mechanism for the formation of ply wrinkles due to shear between plies. Compos A Appl Sci Manuf 2013;49:139–47.
[128] Lightfoot JS, Wisnom MR, Potter K. Defects in woven preforms: formation mechanisms and the effects of laminate design and layup protocol. Compos A Appl Sci Manuf 2013;51:99–107.
[129] Bloom LD, Wang J, Potter KD. Damage progression and defect sensitivity: an experimental study of representative wrinkles in tension. Compos B Eng 2013;45(1):449–58.
[130] Gutowski TG, Dillon G, Chey S, Li H. Laminate wrinkling scaling laws for ideal composites. Compos Manuf 1995;6(3):123–34.
[131] Mathieu S, Hamila N, Bouillon F, Boisse P. Enhanced modeling of 3D composite preform deformations taking into account local fiber bending stiffness. Compo. Sci. Technol 2015;117:322–33.
[132] Boussu F, Cristian I, Nauman S. General definition of 3D warp interlock fabric architecture. Compos B Eng 2015;81:171–88.
[133] Carvelli V, Pazmino J, Lomov SV, Verpoest I. Deformability of a non-crimp 3D orthogonal weave E-glass composite reinforcement. Compos Sci Technol 2012;73:9–18.
[134] Holzapfel G, Gasser T, Ogden R. A new constitutive framework for arterial wall mechanics and a comparative study of material models. J Elast 2000;61:1–48.
[135] Khiêm Vu Ngoc, Krieger Helga, Itskov Mikhail, Gries Thomas, Stapleton Scott E. An averaging based hyperelastic modeling and experimental analysis of non-crimp fabrics. Int J Solid Struct 2017. On line https://doi.org/10.1016/j.ijsolstr.2016.12.018.
[136] Itskov M. On the theory of fourth-order tensors and their applications in computational mechanics. Comput Meth Appl Mech Eng 2000;189:419–38.
[137] Onate E, Zarate F. Rotation-free triangular plate and shell elements. Int J Numer Meth Eng 2000;47:557–603.
[138] Brunet M, Sabourin F. Analysis of a rotation-free 4-node shell element. Int J Numer Methods Eng 2006;66:1483–510.
[139] Mathieu S, Hamila N, Dupé F, Descamps C, Boisse P. Stability of 3D textile composite reinforcement simulations: solutions to spurious transverse modes. Appl Compos Mater 2016;23(4):739–60.
[140] Rahali Y, Goda I, Ganghoffer JF. Numerical identification of classical and non-classical moduli of 3D woven textiles and analysis of scale effects. Compos Struct 2016;135:122–39.
[141] Rahali Y, Ganghoffer JF, Chaouachi F, Zghal A. Strain gradient continuum models for linear pantographic structures: a classification based on material symmetries. J Geom Symmetry Phys 2015;40:35–52.
[142] Rahali Y, Assidi M, Goda I, Zghal A, Ganghoffer JF. Computation of the effective mechanical properties including nonclassical moduli of 2.5 D and 3D interlocks by micromechanical approaches. Compos B Eng 2016;98:194–212.
[143] ElNady K, Goda I, Ganghoffer JF. Computation of the effective nonlinear mechanical response of lattice materials considering geometrical nonlinearities. Comput Mech 2016;58(6):957–79.
[144] Rahali Y, Dos Reis F, Ganghoffer JF. Multiscale homogenization schemes for the construction of second-order grade anisotropic continuum media of architectured materials. Int J Multiscale Comput Eng 2017;15(1).
[145] Spencer AJM, Soldatos KP. Finite deformations of fibre-reinforced elastic solids with fibre bending stiffness. Int J Non Lin Mech 2007;42(2):355–68.
[146] d'Agostino MV, Giorgio I, Greco L, Madeo A, Boisse P. Continuum and discrete models for structures including (quasi-) inextensible elasticae with a view to the design and modeling of composite reinforcements. Int J Solids Struct 2015;59:1–17.
[147] dell' Isola F, Steigmann D. A two-dimensional gradient-elasticity theory for woven fabrics. J Elast 2015;118(1):113–25.
[148] Goda I, Ganghoffer JF. Construction of first and second order grade anisotropic continuum media for 3D porous and textile composite structures. Compos Struct 2016;141:292–327.
[149] Rahali Y, Giorgio I, Ganghoffer JF, Dell'Isola F. Homogenization à la Piola produces second gradient continuum models for linear pantographic lattices. Int J Eng. Sc 2015;97:148–72.
[150] Ferretti M, Madeo A, dell'Isola F, Boisse P. Modeling the onset of shear boundary layers in fibrous composite reinforcements by second-gradient theory. Z Angew Math Phys 2014;65:587–612.
[151] Madeo A, Barbagallo G, d'Agostino MV, Boisse P. Continuum and discrete models for unbalanced woven fabrics. Int J Solid Struct 2016;94:263–84.
[152] Barbagallo G, Madeo A, Morestin F, Boisse P. Modelling the deep drawing of a 3D woven fabric with a second gradient model. Math Mech Solid 2017;22(11):2165–79.
[153] Ahmad S, Irons BM, Zienkiewicz OC. Analysis of thick and thin shell structures by curved finite elements. Int J Numer Meth Eng 1970;2(3):419–51.